STRUCTURAL MODELING AND ELECTRON PARAMAGNETIC RESONANCE SPECTROSCOPY OF THE HUMAN Na^+/H^+ EXCHANGER ISOFORM 1, NHE1

Eva B. Nygaard[§], [,] Jens O. Lagerstedt[#,†], Gabriel Bjerre[§,1], Biao Shi[‡,1], Madhu Budamagunta[†], Kristian A. Poulsen[§], Stine Meinild[§], Robert R. Rigor[‡], John C. Voss[†], Peter M. Cala[‡,*] and Stine F. Pedersen[§,*]

[§]Department of Biology, University of Copenhagen, Denmark, [#] Department of Experimental Medical Science, Biomedical Center, Lund University, Sweden, and Departments of [†]Biochemistry & Molecular Medicine and [‡]Physiology & Membrane Biology, University of California, Davis, California

Running head: Structural modeling and EPR spectroscopy of NHE1

[*]Address correspondence to: Stine F. Pedersen, Department of Biology, Universitetsparken 13, University of Copenhagen, DK-2100 Copenhagen, Denmark, sfpedersen@bio.ku.dk and Peter M. Cala, Dept. of Physiology & Membrane Biology, School of Medicine, University of California Davis, One Shields Ave., Davis, CA 95616; E-mail: pmcala@ucdavis.edu.[1)] Contributed equally to this work.

We previously presented evidence that TM IV and TM X-XI are important for inhibitor binding and ion transport by the human Na^+/H^+ exchanger, hNHE1 (Pedersen et al., J. Biol Chem. 2007, 282:19716-19727). Here, we present a structural model of the transmembrane part of hNHE1 that further supports this conclusion. The hNHE1 model was based on the crystal structure of the *E. coli* Na^+/H^+ antiporter, NhaA and previous cysteine scanning accessibility studies of hNHE1 and was validated by electron paramagnetic resonance (EPR) spectroscopy of spin labels in TM IV and -XI, as well as by functional analysis of hNHE1 mutants. Removal of all endogenous cysteines in hNHE1, introduction of the mutations $Ala^{173}Cys$ (TM IV) and/or $Ile^{461}Cys$ (TM XI), and expression of the constructs in mammalian cells resulted in functional hNHE1 proteins. The distance between these spin-labels was approximately 15 A, confirming that TM IV and -XI are in close proximity. This distance was decreased both at pH 5.1 and in the presence of the NHE1 inhibitor cariporide. A similar TM IV-TM XI distance, and a similar change upon a pH shift were found for the cariporide-insensitive *P. americanus* (pa)NHE1, however, in paNHE1, cariporide had no effect on TM IV-TM XI distance. The central role of the TM IV-TM XI arrangement was confirmed by the partial loss of function upon mutation of Arg^{425}, which the model predicts stabilizes this arrangement. Data are consistent with a role for TM IV and -XI rearrangements coincident with ion translocation and inhibitor binding by hNHE1.

The ubiquitous plasma membrane Na^+/H^+ exchanger isoform 1 (NHE1) plays central roles in cellular pH and volume homeostasis, cell migration, proliferation, and survival, yet increased NHE1 activity contributes to ischemia-reperfusion injury as well as tumor growth and proliferation (1,2). Hence, the ability to selectively block NHE1, while of high clinical relevance, is hampered by a lack of a detailed understanding of NHE1 structure and mechanism of ion translocation.

Hydropathy analyses and accessibility studies suggest that NHE1 has 12 transmembrane (TM) segments, and a large C-terminal cytoplasmic region (3). Cysteine accessibility studies suggest the presence of two small reentrant loops between TM IV and TM V (Intracellular Loop (IL) II) and TM VIII and TM IX (IL IV), respectively and a larger reentrant loop between TM IX and TM X (Extracellular Loop (EL) V) (1,3). Portions of IL II and IL IV are located within the membrane and accessible from either side of the membrane, suggesting that they may form structures lining an aqueous pore and could be involved in ion translocation by NHE1 (3). EL V is also interesting in this regard, as it resembles the P-loops found in e.g. voltage gated ion channels (1,3). These putative reentrant loops are highly conserved among several NHE1 homologs, consistent with the notion that they are critical for NHE1 function (3-5).

A number of regions within the NHE1 protein have been implicated in inhibitor binding, e.g. TM IV and TM IX (6-11), however, the mechanism(s) of interaction between NHE1 and its commonly used inhibitors, amiloride- and benzoyl guanidine

(HOE-) type compounds, remain to be fully elucidated.

Using a comparative approach based on chimeras generated using human NHE1 (hNHE1) and two NHE1 homologs (flounder, paNHE1 and Amphiuma, atNHE1) with high sequence homology to hNHE1, yet markedly different inhibitor profiles (4,5), we previously obtained novel information on the regions of NHE1 important for inhibitor binding and ion transport (12). These studies confirmed that TM IV plays a central role in inhibitor binding (12) as suggested by earlier point mutation studies (6-11). Moreover, we demonstrated that regions in TM X-XI and/or IL V and EL VI are important determinants of inhibitor sensitivity (12).

The three-dimensional (3D) structure of NHE1 is unknown, however the structure of the distantly related bacterial *(Escherichia coli)* Na^+/H^+ antiporter NhaA was recently solved at 3.45 Å resolution (13). Similar to NHE1, NhaA has 12 membrane spanning domains and intracellular N- and C-termini (13). As with NHE1, NhaA is important for cellular pH regulation and electrolyte homeostasis (1). Despite the low sequence homology (<15% similarity as calculated by ClustalW analysis), and different Na^+:H^+ transport stoichiometry (NHE1 = 1:1, NhaA = 1:2), comparison of NHE1 and NhaA is relevant given their similar topology and the fact that structure tends to be far better conserved than sequence. A hNHE1 lacking *N*-glycosylation sites and expressed in *S. cerevisiae*, was recently used to create a 22 Å resolution structure (14). However, as glycosylation is important for NHE1 trafficking (15), it is uncertain whether this structure is representative of the mature NHE1.

The low sequence homology between NhaA and NHE1 makes homology modeling highly challenging. A structural model of hNHE1 based on threading on NhaA has recently been published (16). This model was constructed from multiple sequence alignments, fold recognition, and evolutionary conservation analysis. However, the assignment of TM regions in this model is inconsistent with experimental evidence from earlier cysteine scanning accessibility studies of hNHE1 (3), and the model was not validated by experimental measurements of inter-helix distances in hNHE1.

We have therefore created a 3D structural model of the N-terminal region of hNHE1 based on threading (17) on the NhaA structure, in which we constrained our alignment of TM domains to regions of NHE1 that were experimentally determined to be in a membrane-like environment. In the NhaA structure, and thus in our model, TM IV and TM XI are in close proximity, in agreement with our experimental evidence for hNHE1 (12). The hypothesis that these helices are involved in ion translocation and inhibitor binding by NHE1 was tested (i) through functional analysis of NHE1 mutants and (ii) by experimentally determining the relative positions of TM IV and TM XI and their conformational changes during activation and inhibition. Accordingly, cysteine residues were introduced at the desired positions, followed by addition of site-directed spin labels (SDSL). The labeled protein was then used for electron paramagnetic resonance (EPR) spectroscopy (18). The EPR spectra provide information on side chain dynamics (19), and thus on protein topography and conformational changes, as well as on secondary and tertiary structure (20,21). Introduction of a second paramagnetic center allows distance measurements within the protein (18,21).

We present here a 3D model of hNHE1 threaded on the NhaA structure, in which TM IV and TM XI are in close proximity. EPR analyses of hNHE1 and the *Pleuronectes americanus* homolog, paNHE1, combined with point mutations and NHE1 function analyses confirmed the close proximity of TM IV and -XI and were consistent with a major role for these regions in ion translocation and inhibitor binding by NHE1.

EXPERIMENTAL PROCEDURES

Materials

Unless otherwise stated, reagents were from Sigma-Aldrich or Fisher. Complete™ protease inhibitor was from Roche Diagnostics. Cariporide was a kind gift from Sanofi-Aventis. 5'-(N-ethyl-N-isopropyl) amiloride (EIPA) was from Sigma-Aldrich. *n*-dodecyl ß-D-maltopyranoside (DDM) was from Anatrace. (1-Oxyl-2,2,5,5-tetramethylpyrroline-3-methyl)methanethio-sulfonate (MTS spin-label) was from Toronto Research Chemicals. HiTrap Chelating Nickel column and CaM agarose beads for affinity

chromatography were from GE Healthcare and Sigma-Aldrich, respectively.

Structural Modeling of the N-terminal Domain of hNHE1

The structural homology model of the N-terminal domain of NHE1 protein was generated from its primary sequence (residues 1-507) using several local structure and fold recognition methods at the MetaServer (bioinfo.pl/meta/) (22). The established structure of the protein with the highest scores (NhaA; PDB accession code 1ZCD), as evaluated by the 3D-Jury method at the same server, was used as template and the comparison was done with the Swiss-Model program (23).

Threading of NHE1 on the NhaA template was limited to the N-terminal domain of NHE1 (residues 1 to 507), that includes the membrane-spanning domains. Structurally, the N-terminal domain of NHE1 is distinguished from that of NhaA by a much greater fraction of hydrophilic (extra-membrane) sequence. Thus, nearly all of the assigned structure in the model for NHE1 concerns the transmembrane regions of the protein. We therefore constrained our alignment of NHE1 and NhaA to sequences (and their flanking 10 residues) that have been found experimentally (3) to reside in a membrane-like environment. Alignments between the known NhaA TM regions and the hNHE1 TM regions (including the flanking 10 residues) suggested by Wakabayashi et al. based on cysteine accessibility analyses (3) were then carried out independently using the ClustalW algorithm. The resultant TM alignments were then used to match the regions of low homology and ensure that gaps fell within the hydrophilic loops connecting the TM segments.

Analysis of the NHE1 N-terminal domain structural model was performed by use of DeepView/Swiss-PdbViewer (www.expasy.org/spdbv) and by use of Insight II software (version 2005) on the Octane workstation by Silicon Graphics. Figures were produced using UCSF Chimera software (www.cgl.ucsf.edu/chimera). Calculation of the distance between Ala^{173} and Ile^{461} based on our homology model and that of Landau et al. (16) was made using the same UCSF Chimera software. We are grateful to M. Landau, Tel-Aviv University, Israel, for providing us with the PDB file that allowed us to calculate this value for their model.

Cell Culture

AP-1 cells (a Chinese Hamster Ovary (CHO)-derived cell line with no endogenous NHE activity (24) were a kind gift from Dr. S. Grinstein, Hospital for Sick Children, Toronto, Canada. These cells have previously been shown to exhibit no recovery from an acid load in the nominal absence of HCO_3^- (12,24). AP-1 cells were grown at 37°C, 5% CO_2, 95% humidity in α-minimum Essential medium with Eagle's salts (Meidatech, Inc., Manassas, VA), supplemented with 10% fetal bovine serum, 1% L-glutamine, 1% penicillin/streptomycin and 600 μg/ml Geneticin (G418) sulfate (Invitrogen). Every 3-4 days, cells were passaged by gentle trypsinization, and only passages 5-30 were used for experiments.

Constructs and stable transfection of mutant hNHE1 and paNHE1

The full length Cys-less hNHE1 was constructed by replacing all native cysteine residues with alanines. Using restriction digest, hNHE1 was cloned into the mammalian expression vector pcDNA3.1(+) (Invitrogen). The desired residues were altered using site-directed mutagenesis (QuickChange XL, Stratagene, CA). To facilitate affinity chromatography purification of the constructs, a poly-His tag was added to the C-terminal end by three-way ligation. This Cys-less construct was found to be fully functional, in agreement with earlier reports (3). From the Cys-less construct, three different hNHE1 constructs containing Cys replacements at Ala173 and/or Ile461 were prepared. All constructs were verified by DNA sequencing prior to transfection (DBS Sequencing Facility, University of California Davis). Positive transfectants were selected for resistance to 600 μg/ml G418. hNHE1 expression was verified by immunoblotting as previously described (25). Briefly, protein homogenates were separated on 7.5% SDS-PAGE gels and electrotransferred to nitrocellulose or PVDF membranes. Mouse monoclonal NHE1 antibody (MAB3140 Millipore/Chemicon) or rabbit polyclonal NHE1 antibody (a kind gift from Mark Musch, University of Chicago) and horseradish peroxidase-conjugated goat secondary antibodies were used to label NHE1, followed by visualization by enhanced chemiluminescence (GE

Healthcare). Clonal selection was carried out by limiting dilution, and stably transfected clones were used in all experiments. The corresponding set of constructs for paNHE1, i.e. cysless paNHE1 with reintroduction of cysteines in Ala^{164} (TM4), Ile^{452} (TM11) and Ala^{164}/Ile^{452}, were prepared in a similar manner.

Functional analysis of NHE1 mutants expressed in AP-1 cells

All constructs were tested for NHE1 function using in Zeiss Axiovert S100 microscope or a PTI fluorescence spectrophotometer, employing the pH-sensitive fluorescent probe 2′,7′-bis-(2-carboxyethyl)-5,6-carboxyfluorescein, tetra-acetoxymethylester (BCECF-AM) to monitor intracellular pH (pH_i). We employed the ammonium pre-pulse technique to acid-load the cells, as previously described in detail (12). Isotonic Ringer for pH_i measurements (IR) contained, in mM: 130 NaCl, 3 KCl, 20 HEPES, 1 $MgCl_2$, 0.5 $CaCl_2$, 10 NaOH, 10 glucose; pH 7.4, 300 mOsm.

Immunofluorescence analysis of wild type and mutant NHE1 expressed in AP1 cells

Immunofluorescence labeling of NHE1 in AP-1 cells was carried out as described previously (26). Briefly, cells grown on glass coverslips were washed in isotonic Ringer (in mM: 130 NaCl, 3 KCl, 20 HEPES, 1 $MgCl_2$, 0.5 $CaCl_2$, 10 NaOH, 10 glucose, pH 7.4), fixed in 2% paraformaldehyde, washed in TBS (in mM: 150 NaCl, 10 Tris-HCl, 1 $MgCl_2$, 1 EGTA), permeabilized (0.2% triton X-100 in TBS), blocked in 5% BSA in TBST, incubated with primary antibody against NHE1 (Xb-17, 1:100 in TBST), washed in TBST, incubated with Alexa488-conjugated anti-mouse secondary antibody (1:600 in TBST, 1 h), washed in TBST and mounted. Fluorescence was visualized using a 100 X/1.4 NA plan apochromat objective, pinhole size 1 airy disc, and the 488 nm laser line of a Leica DM IRB/E microscope and Leica TSC NT confocal laser scanning unit (Leica Lasertechnik GmbH, Heidelberg, Germany). Images shown are frame averaged and presented in RGB pseudocolor. No or negligible labeling was detectable in the absence of primary antibody. The relative plasma membrane levels of wt and Arg^{425}Ala hNHE1 were estimated from the NHE1 immunofluorescence images by placing regions of interest arbitrarily in the plasma membrane and cytosolic regions (4 of each per cell), and calculating the mean plasma membrane/cytosolic pixel intensity ratio per cell. Ratios obtained were 1.72 ± 0.110 (wt) and 0.67 ± 0.048 (Arg^{425}Ala), resulting in an estimated relative plasma membrane expression level of 0.67/1.72 = 0.39 (n=12 cells in 3 independent experiments for each cell type).

Expression and functional analysis of Arg^{425}Ala NHE1 in Xenopus oocytes

Expression and functional analysis of hNHE1Arg^{425}Ala was carried out as previously described (27). Briefly, the human Arg^{425}Ala NHE1 was cloned into a vector optimized for oocyte expression (pDEST SML). The cDNA was linearized and *in vitro* transcribed with T7 RNA polymerase using the T7 mMessage mMashine Kit (cat. # AM1344, Ambion). 50 ng of cRNA was injected into defoliculated *X. laevis* oocytes, which were incubated in Kulori medium (in mM: 90 NaCl, 1 KCl, 1 $CaCl_2$, 1 $MgCl_2$, 5 HEPES, pH 7.4) at 19°C for 3–7 days before experiments were performed. The two-electrode voltage clamp method was used to control the membrane potential and monitor the current in oocytes expressing Arg^{425}Ala hNHE1. The recordings were performed at room temperature with a Dagan clampator interfaced to an IBM compatible PC using a DigiData 1320 A/D converter and pCLAMP 9.0 (Axon Instruments). Currents were low pass-filtered at 500 Hz and sampled at 2 kHz. Electrodes were pulled from borosilicate glass capillaries to a resistance of 0.5–2 megaOhm and were filled with 1 M KCl. Generally, the membrane potential (V_m) was held at -50 mV and the experimental chamber was continuously perfused by a NaCl buffer (in mM: 100 NaCl, 2 KCl, 1 $CaCl_2$, 1 $MgCl_2$, 10 HEPES, pH 7.4). The I/V relations were obtained by changing the membrane potential from +50 to -150 mV in 20 mV increments and measuring the resulting steady state current at each membrane potential. The I/V relationships were obtained in the NaCl buffer at normal pH (pH 7.4) and at low pH (pH 5.8) and in Na^+ free buffers (as above but with 100 mM Na^+ exchanged with 100 mM NMDG-Cl) at the two pH-values. The actual I/V curves were obtained by subtracting currents in NMDG-Cl buffer from

currents obtained in NaCl buffer. To stimulate NHE1, oocytes were incubated for 60 min in the low pH buffer before the I/V relationships were determined.

Preparation of membrane fractions

Preparation of membrane fractions was based on (14), with several modifications. Unless otherwise indicated, subsequent procedures were carried out at 4°C. One day post-confluence, cells were washed in PBS (in mM: 60 K_2HPO_4, 30 KH_2PO_4, 145 NaCl, pH 7.5) and harvested in lysis buffer (in mM: 25 HEPES, 1 EGTA, 1 EDTA, 1 PMSF, pH 7.5) containing a protease inhibitor cocktail (Complete™, Roche Diagnostics). The cells were pelleted, resuspended in 4 ml lysis buffer and complete lysis was obtained by sonication. Lysates were centrifuged at 6000×g (15 min) and the supernatant (S1) saved. The pellet was resuspended in lysis buffer, centrifuged at 7500×g (10 min) and the supernantant (S2) combined with S1. S1 + S2 were centrifuged at 150,000 g (60 min), and the pelleted membrane fractions resuspended in lysis buffer (in mM: 25 HEPES, 1 EGTA, 1 EDTA, 1 PMSF, pH 7.5) containing protease inhibitor, snap frozen in liquid nitrogen and stored at -80°C. The membrane fraction was diluted with stripping buffer (in mM: 25 HEPES, 1750 KCl, 1 EGTA, 1 EDTA, 1 PMSF, pH 7.5) containing protease inhibitor to a final KCl concentration of 0.7 M, incubated at 4°C for 30 min, and the stripped membrane fraction pelleted by centrifugation at 175,000 g (30 min). To solubilize NHE1, pellets were resuspended in solubilization buffer (25 mM HEPES, 100 mM NaCl, 1 mM PMSF, 2% Fos-Cholin 14, 1% Triton X-100, 0.05% DDM, pH 7.5) with EDTA-free protease inhibitor (Complete™ protease inhibitor EDTA-free, Roche Diagnostics) and incubated with mild stirring at room temperature (2×15min). The suspension was centrifuged at 150,000 g to pellet debris (30 min) and the supernatant used for further purification.

Protein purification and spin labeling

To obtain highly purified NHE1, two sequential purification steps were employed. First, a HiTrap Chelating Nickel column was charged with Ni^{2+} according to the manufacturer's protocol and equilibrated with binding buffer (BB, in mM: 25 HEPES, 100 NaCl, 5 imidazole, 0.05% DDM, pH 7.5). The membrane protein extract was applied to the column at 1.0 ml/3 min. The column was subsequently washed with 3 volumes of BB containing 0.05% Triton X-100, and 6 volumes of BB without Triton X-100, at a flow rate of 1 ml/min. Spin labeling was carried out by applying 3 volumes BB containing 0.2 mM MTS spin-label to the column containing bound NHE1 protein (for the use of MTS-SL labels for EPR measurements, see Discussion). The MTS-SL chemically modifies the engineered cysteines by forming covalent interactions with the thiol group on the cysteine side chains. The on-column labeling procedure with bound and enriched target protein allows for efficient labeling and facilitates the subsequent removal of unreacted MTS-SL label. After 30 min of MTS labeling, the column was extensively washed with BB and washing buffer (as BB but with 50 mM imidazole) to remove unreacted MTS-SL, then eluted with elution buffer (as BB but with 300 mM imidazole) at 1 ml/3 min. The eluates were collected for further purification according to OD 280 measurements. In the second purification step, 1.5 ml of CaM-agarose affinity resin was pre-equilibrated by rocking for 10 min in 6 ml of CaM binding buffer (CaM-BB, in mM: 25 HEPES, 100 NaCl, 2.5 $CaCl_2$, 2.5 $MgCl_2$, 0.05% DDM, pH 7.5) 2 to 3 times. To allow NHE1 protein to bind to the CaM resin, the eluted sample from the nickel column was incubated with the resin in the presence of 2.5 mM $CaCl_2$ and 2.5 mM $MgCl_2$ for 1 h at room temperature. The column was washed 4 times with 6 ml CaM-BB and once or twice with 6 ml of HEPES buffer (25 mM HEPES, 100 mM NaCl, 0.05% DDM). To elute NHE1 from the CaM resin, the washed resin was rocked in 2.5 ml of CaM elution buffer (CaM-EB, in mM: 25 HEPES, 100 NaCl, 2.5 EGTA, 2.5 EDTA, 0.05% DDM, pH 7.5) containing 0.1 mM of the CaM binding domain (494-513) of eNOS for 1 h at room temperature and overnight at 4°C. The eluates were collected, and the column was further eluted with 1.6 ml of CaM-EB containing 0.05 mM eNOS peptide and 0.05% of FC-14 by rocking for 1 h at room temperature and 1.5 h at 4°C. The two eluates were pooled and concentrated to 40-60 µl (from ~4 ml), using a 30 kD Vivaspin 2 concentrator (Vivascience).

Coomassie Fluor Orange Staining

The presence of hNHE1 in each purified

protein sample was confirmed by immunoblotting as described above, and the purity was assessed by Coomassie Fluor Orange Protein Gel Staining according to the manufacturer's (Invitrogen/ Molecular Probes) protocol. Briefly, a minigel was incubated with 100 ml of the staining solution by rocking for 45 min. The stained gel was washed first with 7.5% acetic acid solution briefly, then with water for 5 min once or twice. The gel was imaged using a Fujifilm Imager LAS-4000.

Functional analysis of reconstituted hNHE1

Reconstitution of NHE1 protein- Purified poly-histidine tagged NHE1 protein was reconstituted into liposomes formed of *E. coli* polar lipids (Avanti Polar Lipids, Inc., Alabaster, AL) essentially as in (28,29) Briefly liposomes to be assayed for either $^{22}Na^+$ uptake or H^+ flux were mixed in a protein:lipid ratio of 1 µg:mg or 5 µg:mg, respectively. Lipids were prepared by nitrogen streaming to dryness, washed in pentane, and reconstituted in appropriate intravesicular buffers (for $^{22}Na^+$ uptake: 400 mM NaCl, 10 mM MES at pH 6.0; for H^+ flux: 300 mM KCl, 100 mM citrate, 40 mM KH_2PO_4, pH 4.0). 34 mM CHAPS was added to uniform opacity under sonication, followed by a 1 h preincubation before adding NHE1 protein. Vesicles were gel filtered with sephadex beads saturated with intravesicular buffer, and eluted with the same buffer. Vesicle-containing fractions were snap-frozen in liquid nitrogen and stored at -80°C in 110 µl aliquots.

$^{22}Na^+$ uptake or H^+ flux in reconstituted liposomes- For $^{22}Na^+$ uptake assays, liposomes were centrifuged at low-speed through extravesicular medium (EVM1: 10 mM MES, 800 mM sucrose/sorbitol, pH 6.0) saturated sephadex beads as in (28), suspended in 100 µl EVM1, and immediately combined with 700 µl EVM1 containing $^{22}Na^+$ (0.5 µCi/ml). 100 µl aliquots were sampled by washing through DOWEX cation exchange resin with 15 volumes of cold EVM1. Sample γ radioactivitity was quantified by Cerenkov counting. Valinomycin permeabilization was used to obtain isotope saturation of the liposomes, and empty liposomes were used to obtain non-specific $^{22}Na^+$ uptake (subtracted as background). For H^+ flux assays, liposomes were washed in a similar fashion with sephadex (EVM2: 0.3 mM HEPES, 400 mM KCl, pH 7.4) and 100 µl removed to a small glass chamber with a micro-stir bar. A pre-calibrated pH microelectrode (Microelectrodes, Inc., Bedford, NH) was placed into the solution, under continuous sampling to a PowerLab data acquisition system (ADInstruments, Inc., Colorado Springs, CO), and the solution was adjusted to 7.4. 10 µl poorly buffered NaCl solution (4 M NaCl, 0.3 mM HEPES) was added to initiate H^+ flux. H^+ flux was determined by conversion and correction for the measured buffer capacity of EVM2. In both assays, liposomes treated with inhibitor were suspended in EVM in presence of 50 µM EIPA.

EPR spectroscopy

EPR measurements were performed using a JEOL X-band spectrometer fitted with a loop-gap resonator (30,31). A 6 µl aliquot of the purified, spin-labeled protein, at a final concentration of approximately 10 µM (1.0 µg/µl) in CaM elution buffer (pH 7.5) containing 0.01% DDM, was placed in a sealed quartz capillary contained in the resonator. Spectra (averages of three 2-min scans) were acquired at room temperature at a microwave power of 4 mW and with the amplitude optimized to the natural line width of the individual spectrum. Spectra were normalized according to their double integrated intensity. To narrow the broaden spectra and improve integration quality, normalization was performed on each sample in the presence of SDS (2% final). After the double integration, the total area was equalized for the two single-labeled constructs, TM IV ($Ala^{173}Cys$) and TM XI ($Ile^{461}Cys$), respectively, which thus normalized them to the same number of spins. The spectra of the two single-labeled constructs were summed, and compared to the spectrum for the double-labeled construct, using the same process as described above. The identically treated Cys-less protein that was used as a negative control does not provide a signal above background (Fig. 6, pink trace).

RESULTS

Structural model of hNHE1

In order to create the tertiary structural model of the transmembrane N-terminal domain of hNHE1 we used *in silico* homology structure building, using the known structure of NhaA as a template. The primary structure of the N-terminal domain (residues 1 to 507) of hNHE1 was analyzed for structural homologs at the

MetaServer (bioinfo.pl/meta/) (22). Despite low primary sequence identity, substantial structural similarities between hNHE1 and NhaA (PDB accession code 1zcd) were identified.

Based on previously published experimental findings (3) and sequence analysis, the primary sequence alignment was manually optimized prior to threading the hNHE1 sequence onto the NhaA tertiary structure (Fig. 1). The resulting structural homology model of hNHE1 (Fig. 2) is limited to the N-terminal (largely membrane spanning) domain and encompasses amino acid residues Pro^{12} to Ala^{507}. In accordance with the general finding that prokaryotic membrane proteins possess shorter extramembrane loops and terminal extensions than eukaryotic members of the same superfamily (see (32), NhaA is seen to have smaller extra-membrane loops than NHE1 (Fig. 1). Consequently, several of the intra- and extra-cellular loops connecting the transmembrane regions were excluded from our model of hNHE1 (see also Experimental Procedures). In the NhaA structure, and thus in our model, TM IV and TM XI are in close proximity (Fig. 2 and close-up view in Fig. 4). It is noteworthy that the architecture and antiparallel arrangement of TMs IV and XI are unusual in that both helices are extended and positioned such that the partial charges of the N-terminal and C-terminal dipoles are in close apposition, in the membrane interior. Closer examination of the threaded model allowed us to identify amino acid residues that are important elements of the putative catalytic core of hNHE1 (Figs. 3 and 4). Briefly, from the solid surface representation of the hNHE1 model shown in Fig. 3A-B it is clearly seen that several charged and polar residues are located near this cavity. Importantly, Arg^{425} (corresponding to Lys^{300} in NhaA, which is assigned a central role in the catalytic core of NhaA; see reference 13) and presumably then that of NHE1, is accessible from the cytoplasmic side, despite being positioned approximately in the central plane of the lipid bilayer. Fig. 3C shows a side view of the model, illustrating that primarily hydrophobic side chains are pointed into the interior of the lipid bilayer.

Functional analysis of Cys-replaced mutants and reconstituted NHE1 protein

The residues Ala^{173} and Ile^{461} were chosen for cysteine replacements for site-directed spin labeling, because of their locations in TM IV and TM XI, respectively, which have been assigned important roles in ion translocation (Fig. 4). Importantly, the conservation of these residues between NHEs is low, and replacement was therefore not likely to interfere with protein function.

To ascertain that the introduction of cysteines at these positions had not compromised NHE1 function, which would render inter-helix distance measurements unreliable, the function of each construct was tested after expression in AP-1 cells, by monitoring pH_i recovery after acidification induced by a NH_4Cl prepulse. As seen in Fig. 5A-C, the three Cys-replaced constructs ($Ala^{173}Cys$, $Ile^{461}Cys$, and $Ala^{173}Cys/Ile^{461}Cys$) were all functional and their regulation by pH_i appeared normal. It is noteworthy that this contrasts with a previous study in which an $Ala^{173}Cys$ mutation was found to reduce NHE1 function (33). The reason for this discrepancy is not clear, however, it may be significant that virtually all Cys mutants studied by Slepkov and coworkers (33) exhibited strongly reduced function, including L^{163} and G^{174}, whereas comparable mutations have been reported by others to be fully functional (34). Similarly, all the corresponding paNHE1 constructs were fully functional (not shown, n=2-3 independent experiments per condition).

Fig. 5D shows a representative Coomassie Fluor Orange stain and corresponding Western blot of an $Ala^{173}Cys/Ile^{461}Cys$ hNHE1 sample purified for EPR. As seen, the final eluted sample is highly enriched in NHE1 protein. While the final eluate is greatly purified compared to the starting material, it contains several bands as revealed by Coomassie Fluor Orange staining. However, comparison of the Western blot and Coomassie data strongly indicates that the majority of the protein in the sample is NHE1: the ~100 and ~85 kDa bands correspond to glycosylated and immature NHE1, respectively, and the ~200+ kDa smear is likely to be NHE1 dimers or oligomers.

Another concern was whether the purification and reconstitution of NHE1 might affect function. We therefore monitored NHE1 function following reconstitution in liposomes, i.e. a treatment and environment similar to those of the EPR experiments. As illustrated in Fig. 5E-F, acid-activated H^+ and Na^+ transport sensitive to the

NHE1 inhibitor EIPA was clearly evident following NHE1 reconstitution. That NHE1 was functional after purification and reconstitution is a strong indicator that, in our hands, structure was preserved. A third possible caveat would be if spin labeling significantly altered protein folding, stability or behavior. However, this is highly unlikely to be the case to any detectable extent (see Discussion).

EPR analysis supports the structural model of hNHE1

EPR line-shape of single-labeled hNHE1- As noted above, it is necessary to obtain EPR analyses of the non-interacting individual spin-labeled proteins in order to measure the distance between two spin-labels. Hence, hNHE1 constructs with single-labeled TM IV ($Ala^{173}Cys$) and single-labeled TM XI ($Ile^{461}Cys$), respectively, were purified, labelled, and analysed by EPR. Unless otherwise stated, these analyses were performed at pH 7.5, i.e. under conditions where NHE1 is expected to be in its inactive conformation. Comparison of the EPR spectra of the two single-labeled constructs reveals different spectral shapes (Fig. 6B, top). The spectrum for the single-labeled TM IV ($Ala^{173}Cys$) construct exhibits less broadening, compared to the single-labeled TM XI construct ($Ile^{461}Cys$), which displays a strongly immobilized component in the low field peak. This reflects that position 173 experiences greater motional freedom, possibly arising from a more disordered backbone. Since the presence of trace amounts of proteins other than NHE1 in the purified sample cannot be ruled out (see Fig. 5D), an important control is the EPR signal from the Cys-less NHE1, which was purified and labeled in exactly the same manner as the remaining samples. This is the background signal, a minor contribution that was subtracted from the signal for each of the Cys-containing mutants (Fig. 6).

Distances measurements between the two spin-labels on TM IV and TM XI, respectively- The EPR spectrum for the double-labeled TM IV/TM XI construct containing spin-labels at residues 173 and 461 is shown in Fig. 6B, bottom, black traces. In the absence of spin-spin interaction in the double-labeled construct, the spectrum would approximate the spectral sum of the two corresponding single-labeled constructs. However, when comparing the trace for the double-labeled versus the sum of the single-labeled constructs, the latter shows less spectral broadening (Fig. 6B), indicating a dipolar component in the double-labeled sample. Since dipolar broadening of spin-labeled proteins is only appreciable for distances within 20 Å *(35)*, the moderate level of broadening seen here is consistent with nitroxide moieties separated by a distance on the order of 13-17 Å, assuming a narrow distribution of distances separating the spin pairs (18,36,37) Given the low expression levels of the proteins in cell culture, and the low purification yield, the limited signal:noise ratio of the EPR spectra makes the quantitative calculation of the interspin distance unreliable. However, a qualitative determination within ± 2 Å is sufficient for the identification of neighboring TM domains.

Effect of the functional state of hNHE1 on the distance between TM IV and TM XI- The double-labeled construct was next studied to observe whether manipulations shown to activate or inhibit the protein result in positional changes in TM IV and TM XI as reflected in altered interaction between the spin labels. Reducing buffer pH to 5.1, which is expected to activate hNHE1 (yet which may also exert inhibitory effects due to competition with Na^+; see Discussion), induces a significant additional broadening of the spectrum for the double-labeled construct resulting in the apparent reduction of its signal height (Fig. 6B, bottom left, green trace). This indicates that the distance between residues 173 and 461 of hNHE1 is reduced in the acidic buffer. Similarly, addition of 10 μM of the NHE1 inhibitor cariporide to the purified protein also increases the spectral broadening (Fig. 6B, bottom left, red trace). As the lowered pH, the inhibitor therefore induces a conformation where the two positions experience stronger interaction, although still within the intermediate regime for dipolar coupling (13-17 Å). The inhibitory effect of cariporide on NHE1 function in AP-1 cells is shown in Suppl. Fig. 1.

Analysis of TM IV-TM XI distance and dynamics in paNHE1- If the TM IV-TM IX complex conserved from NhaA to NHE1 is central to ion translocation by NHE1, then these helices should also be in similarly close proximity in NHE1 from other vertebrate species.. Moreover, if the effect of cariporide seen in Fig. 6B indeed reflects interaction of the inhibitor with NHE1, it should

not be seen in the flounder protein (paNHE1), which we have previously shown to be insensitive to cariporide (12). We therefore carried out the corresponding experiment in paNHE1, which shares high sequence homology to hNHE1 in both regions. Thus, all endogenous cysteines were removed, and Cys substituted at the corresponding TM IV or TM XI location. In paNHE1 these positions are Ala^{164} (TM IV) and Ile^{452} (TM XI). Likewise, the double Cys mutant (Ala^{164}/Ile^{452}) was also generated to determine the proximity of TMs IV and XI. The EPR analysis of the spin-labeled paNHE1 protein is shown in Figure 7. As seen in Fig. 7, the two single-labeled constructs behaved similar to the corresponding hNHE1 constructs, i.e. the spin label in TM11 exhibited greater mobility compared to that in TM4. Similarly, the spectrum for the double-labeled construct was clearly broadened compared to the sum of the two single-labeled spectra (Fig. 7B, bottom), confirming the finding from the hNHE1 experiments that the two helices are close to one another (on the order of 15 Å). The effects of acidic pH and cariporide on the EPR spectrum of the double-labeled paNHE1 are shown in Fig. 7B, bottom left. As illustrated, acidic pH (green trace) resulted in broadening of the spectrum, i.e. the same effect seen for hNHE1. In marked contrast, cariporide (10 μM, red trace) had no detectable effect on the paNHE1, consistent with the lack of functional effect of cariporide on this NHE1 homolog (12).

Collectively, the EPR data thus indicate that spin labels placed approximately in the center of TM IV and TM IX of NHE1 are within 20 Å of each other and that the distance between these spin labels is affected by acidification and by cariporide binding, the latter in the cariporide-sensitive NHE1 homolog only.

Effect of a neutralizing mutation in the putative screen residue Arg^{425}

As alluded to above, the NhaA model suggests that Lys^{300} plays a central role as a "screen residue" that permits the energetically unfavorable dipole-dipole arrangement of the catalytic core of NhaA (13). The corresponding residue in hNHE1 is Arg^{425}, which in the homology model is positioned approximately in the central plane of the lipid bilayer, yet accessible from the cytoplasmic side (see Fig. 3 and 4). We therefore hypothesized that replacement of Arg^{425} with a neutral amino acid residue would destabilize the catalytic core and strongly affect NHE1 function. Introduction of an Arg^{425}Ala mutation indeed reduced NHE1-dependent pH_i recovery after an acid load (Fig. 8A-B). Confocal imaging verified that this at least in part reflected a strongly reduced targeting of the mutant NHE1 to the plasma membrane (Fig. 8C).

One possible effect of the Arg^{425}Ala mutation that would not have been picked up in the pH_i recovery measurements is a switch of the ion transport mode of NHE1 from one of Na^+/H^+ exchange to conductive Na^+ transport. To test this possibility, we expressed the Arg^{425}Ala mutant in *Xenopus* oocytes, allowing us to monitor mutant-related Na^+ currents. In the series of experiments performed, we were unable to distinguish currents in the NHE1-Arg^{425}Ala mutant injected oocytes from those of the non-injected oocytes (Suppl. Fig. 2). It should be noted, that the voltage-dependent currents exhibited substantial variation, most likely due to batch dependent endogenous Cl^- and K^+ channel activity (38,39). Thus, Arg^{425} appears to serve a crucial function in stabilizing NHE1 structure, but its mutation to alanine does not seem to induce a Na^+ current via NHE1.

DISCUSSION

Based on the crystal structure of NhaA (13) and experimental evidence from cysteine accessibility studies (3), we created a threaded structural model of hNHE1. The TM IV/TM XI complex of NhaA, by virtue of its unlikely architecture (charges and partial charges in the membrane interior) and its apparent conservation in NHE1, suggests that it may be the catalytic core of the ion translocation pathway (13). If this inference is correct, it is likely that NHE1 and NhaA mediate Na^+ and H^+ translocation through a very similar mechanism. The inferred structural model of hNHE1 resembles that recently proposed by Landau et al. (16) in many respects. The two models agree on the location of several of the helical transmembrane domains. In addition, the NhaA crystal structure indicates a critical role for a basic side chain on TM X, and both predictions identify Arg^{425} as the residue occupying this position. To further compare the two models, we calculated the distance between the ends of the amino acid side chains of Ala^{173} and Ile^{461} obtained for each model.

This value was very similar for the two models, with a distance of 8.46 Å obtained for our model, compared to 7.91 Å for the Landau model. However, there are significant differences between the TM assignments in the two models. Because of the very low homology of NHE1 to NhaA, we constrained our alignment of TM segments to regions of NHE1 that were experimentally determined (3) to be in a membrane-like environment, whereas Landau et al. (16) achieved their alignment solely from homology-based predictions. For example, the first TM segment in our model starts at residue 15. In contrast, the N-terminal extension in the Landau model is more than 100 residues longer and the first TM segment instead starts at residue 128 (TM I of the Landau model co-localizes with TM III of the structure we propose). This arrangement, however, does not appear to take into account that residues 126 and 127 have previously been shown to be inaccessible for MTSET labeling even in permeabilized cells, strongly indicating that they are embedded in the bilayer (3). Consequently, the negatively charged, or polar, residues facing the ion binding pocket are different in the two models, with Asp^{172} and Thr^{197} (Fig. 4) being postulated to be part of the critical residues for translocation in our model, whereas Landau et al. (16) depict Asp^{238} and Asp^{267} (on TM IV and TM V, respectively, in the Landau model) to provide the negative charges in the core of the translocation pathway. Furthermore, the PX_3D motif is highly conserved in all NHE proteins, and multiple hydropathy and experimental analyses has placed this motif in TM segment IV (e.g. (3,7,25,40). The NhaA structure highlights the significance of this motif, as it facilitates a distinctive extension and crossover of TM domains IV and XI. In our alignment, this motif is assigned to TM IV in agreement with previous experimental evidence (3,40) whereas in Landau et al. (16) this motif falls within TM II. Moreover, in the Landau model, residue 173 (located in TM II in their model) is much farther apart from residue 461 than the distance that we observed experimentally using EPR (approximately 15 Å). Thus, while further validation of both models is obviously needed, the model that we present here is supported by multiple lines of experimental evidence.

Validation of the structural model and ion translocation hypothesis by SDSL and EPR- Our structural model of hNHE1 thus supported our recent evidence that TM IV and TM XI play important roles in inhibitor binding and ion translocation by NHE1 (12). We further validated this notion, first by determining the distance between TM IV and TM XI and the conformational changes in these domains in response to manipulations known to activate or inhibit hNHE1 and paNHE1 by SDSL and EPR spectroscopy. Demonstrating the feasibility of this approach for assessing NHE1 structure, a recently published study employed EPR spectroscopic distance measurements between spin labeled side chains on two NhaA monomers to confirm NhaA dimerization (41). To estimate TM IV-TM XI distances in hNHE1, we created two single-labeled mutants, $Ala^{173}Cys$ and $Ile^{461}Cys$, and the double-labeled mutant, $Ala^{173}Cys/Ile^{461}Cys$. It may be noted that although a strict kinetic analysis was not performed, the function of these constructs was comparable to that of normal hNHE1. Comparison of the spectra for the two single-labeled constructs indicates that residue 173 is in a less constrained environment than residue 461 (Figs. 6-7). This is recapitulated in the model structure, where both residues face the inside of the protein, yet Ile^{461} seems to be more enclosed in the protein than Ala^{173}. The distance between Ala^{173} in TM IV and Ile^{461} in TM XI obtained from the double- and single-labeled constructs was determined to ~15 Å, confirming that TM IV and TM XI are in close proximity.

When pH was reduced to 5.1, the $Ala^{173}Cys/Ile^{461}Cys$ spectrum revealed stronger interaction of the spin-labels, indicating that in this, presumably active, conformation, the spin-labeled side-chains undergo stronger dipolar coupling, although still within the intermediate regime of 13-17 Å (18,36,37). Similarly, in the presence of the NHE1 inhibitor cariporide, the $Ala^{173}Cys/Ile^{461}Cys$ spectrum exhibited increased spin-label interaction. This indicates that interaction of cariporide with hNHE1 causes a conformational change resulting in decreased distance between Ala^{173} and Ile^{461}. Again, this would be in congruence with our recent findings that TMs IV and XI play a key role in inhibitor binding and therefore are strong candidate domains for participation in the ion translocation process (12). EPR analysis of the corresponding set of residues in the cariporide-insensitive

paNHE1 homolog showed that the spin label distance as well as the effect of acidification were similar to those observed for hNHE1, while introduction of cariporide had no effect on the EPR spectrum. This difference in the effect of cariporide on the distance between TMs IV and XI in hNHE1 and paNHE1 shows that the TM IV – XI complex is conserved among vertebrate NHE1s, and provides a strong indication that the effect of cariporide on the EPR spectrum in fact reflects an inhibitory interaction of this compound with the transporter.

These findings correlate very well with the NhaA translocation mechanism proposed by Hunte et al. (13). In the NhaA structure (and thus in our hNHE1 model), the TM IV/TM XI helices are extended, cross over each other and exhibit similar conformational changes in response to activating stimuli. Given the homology between the presumed catalytic core in NhaA and NHE1, an equivalent mechanism for ion translocation in hNHE1 seems highly probable. Specifically, Asp^{133} of NhaA aligns with Asp^{172} of hNHE1, Asp^{163} of NhaA aligns with Thr^{197} of hNHE1, and Lys^{300} of NhaA aligns with that of Arg^{425} of hNHE1 in our model (Fig. 4). Asp^{163} of NhaA is suggested to act as a molecular switch, such that its protonation state determines whether the Na^+ binding site (Asp^{164}) is accessible to the periplasm or the cytoplasm (42). In hNHE1, Thr^{197} is likely to carry out the same function as an accessibility-control site. In the NhaA structure, the energetically unfavorable negative/negative and positive/positive dipole-dipole pairings due to the antiparallel extended arrangement of the TM IV/TM XI helices are stabilized by electrostatic screening provided by the negative Asp^{133} and the positive Lys^{300} (13). These residues are conserved among bacterial NhaA homologs and have been shown to be essential to NhaA activity (43,44). We hypothesized that the corresponding residues in hNHE1, Asp^{172} (negative charge) and Arg^{425} (positive charge) fulfill similar dipole ”screening” functions (Fig. 9). If this is correct, a mutation in one of the “screening” residues should severely disrupt the catalytic core of hNHE1. Arg^{425} is located in TM X, which we in our previous studies implicated in ion transport and inhibitor binding (12), and which has been assigned as central in ion translocation by NhaA (44). Moreover, in our structural model, Arg^{425} is located at the bottom of the open cavity and is thus directly accessible from the cytoplasmic side of the membrane (Fig. 3). Consistent with the hypothesis, an Arg^{425}Ala mutation in hNHE1 resulted in marked reduction in NHE1 plasma membrane targeting and pH regulatory ion transport. Our data indicate that membrane targeting of NHE1 is more strongly affected by the Arg^{425}Ala mutation than its transport function. However, regardless of which of these defects is more prominent, they support the hypothesis that Arg^{425} is of central importance in the functionally organized NHE1 protein.

Furthermore, we hypothesize that Arg^{425} not only stabilizes the helices by screening the partial charges from the dipoles on the extended helix C-terminal ends but functions as a "check valve" permitting Na^+ coordination and or gating (Fig. 9). While Arg^{425} on TM X is clearly well positioned for screening the negative dipoles at the C-terminal breaks in TMs IV and XI, intuitively, it seems that this charge-screening role could also be fulfilled through a basic residue in the extended region of TM XI (similar to Asp^{172}). However, the cross-over structure of TMs IV and XI constrains the degree to which this positive charge can be repositioned during the transport cycle. On the other hand, the localization of Arg^{425} along the straight TM X permits axial rotations that can alter the proximity of this charge relative to the catalytic core by several angstroms. In this regard, we postulate that Arg^{425} may function as a gate controlling Na^+ transport.

Critical assessment of the validity of the EPR data- Functional analysis of both Cys-replaced NHE1 mutants in AP-1 cells, and of purified and reconstituted NHE1 protein strongly indicated that NHE1 function, and hence structure, was retained during protein purification and modification for EPR analyses. Another obvious concern in SDSL-EPR experiments is that engineering cysteine substitutions and subsequent modification by the spin label may significantly alter protein folding, stability or behavior. However, substantial work has revealed that the nitroxide ring is well tolerated in proteins and assumes a limited number of rotamers, facilitating the modeling of the spin label within the 3D structure (19,45,46). The method has been applied to a wide assortment of protein types, with very few examples showing a major functional or structural consequence resulting from this modification. Direct evidence

for how the incorporated nitroxide is accommodated in protein structures has been obtained in high-resolution crystal structures of T4 lysozyme containing spin-labeled side chains. Even at buried sites, no significant perturbation of the backbone is evident (19,45). Finally, others have reported modest or negligible effects of spin labeling on protein folding (47) or backbone structure of peptides as measured by NMR (48). This can be attributed to the relatively compact size of the modified Cys residue (a molecular volume on the order of Tyr) and its ambivalent chemical nature, which does not favor highly polar or nonpolar environments. Distortions of a few Å are possible, however, as confidence within ± 5 Å is more than enough to map the correct TM arrangement, this should not cause concern.

Possible mechanism of H^+ sensing by NHE1- In NhaA, TM IX is located at the entrance of the cytoplasmic funnel, where it has been proposed to function as a "pH-sensor" (13). This arrangement is recapitulated in our hNHE1 model (Fig. 9) based upon NhaA crystal structure, our chimera and EPR studies. Thus, the mechanism of pH-regulated ion translocation proposed for NhaA could also be expected for hNHE1 (Fig. 9): an acidic pH change could result in alteration of the protonation state of the region of TM IX located at the entrance of the proposed funnel, which could elicit a conformational change in TM IX, causing a direct contact between TM IV and TM IX. This rearrangement of TM IV could result in a reorientation of the TM IV-TM XI arrangement such that a Na^+ binding site is exposed to the extracellular space. Binding of Na^+ would cause a charge imbalance that would trigger a movement of the TM IV- and TM XI helices, exposing Na^+ to the cytoplasm. The release of Na^+ would result in protonation of the Na^+ binding site, causing a conformational change leading back to the original arrangement of TM IV and TM XI (Fig. 9). At least in NhaA, this mechanism only requires small conformational changes of the helices (13), thus the proposed TM IV/TM XI arrangement would be suited for relatively high turn-over rate of Na^+/H^+ exchange.

In conclusion, we present here a structural model of hNHE1, which places TM IV and TM XI in close proximity. This architecture was confirmed by EPR analyses, from which the distance between TM IV and TM XI was determined at ~15 Å. This distance was decreased and increased, respectively, under conditions of NHE1 activation and inhibition, consistent with a role for TM IV and TM XI rearrangements in ion translocation and inhibitor binding by hNHE1.

REFERENCES

1. Orlowski, J. and Grinstein, S. (2004) *Pflugers Arch.* **447,** 549-565
2. Pedersen, S. F., O'Donnell, M. E., Anderson, S. E., and Cala, P. M. (2006) *Am J Physiol Regul. Integr. Comp Physiol* **291,** R1-25
3. Wakabayashi, S., Pang, T., Su, X., and Shigekawa, M. (2000) *J. Biol. Chem.* **275,** 7942-7949
4. McLean, L. A., Zia, S., Gorin, F. A., and Cala, P. M. (1999) *Am. J. Physiol* **276,** C1025-C1037
5. Pedersen, S. F., King, S. A., Rigor, R. R., Zhuang, Z., and Cala, P. M. (2003) *Bull. Mt. Desert Island* **42,** 38-39
6. Counillon, L., Franchi, A., and Pouyssegur, J. (1993) *Proc. Natl. Acad. Sci U. S. A* **90,** 4508-4512
7. Khadilkar, A., Iannuzzi, P., and Orlowski, J. (2001) *J. Biol. Chem.* **276,** 43792-43800
8. Touret, N., Poujeol, P., and Counillon, L. (2001) *Biochemistry* **40,** 5095-5101
9. Noel, J., Germain, D., and Vadnais, J. (2003) *Biochemistry* **42,** 15361-15368
10. Orlowski, J. and Kandasamy, R. A. (1996) *J. Biol. Chem.* **271,** 19922-19927
11. Wang, D., Balkovetz, D. F., and Warnock, D. G. (1995) *Am J Physiol* **269,** C392-C402

12. Pedersen, S. F., King, S. A., Nygaard, E. B., Rigor, R. R., and Cala, P. M. (2007) *J Biol Chem.* **282,** 19716-19727

13. Hunte, C., Screpanti, E., Venturi, M., Rimon, A., Padan, E., and Michel, H. (2005) *Nature* **435,** 1197-1202

14. Moncoq, K., Kemp, G., Li, X., Fliegel, L., and Young, H. S. (2008) *J Biol Chem.* **283,** 4145-4154

15. Coupaye-Gerard, B., Bookstein, C., Duncan, P., Chen, X. Y., Smith, P. R., Musch, M., Ernst, S. A., Chang, E. B., and Kleyman, T. R. (1996) *Am. J Physiol* **271,** C1639-C1645

16. Landau, M., Herz, K., Padan, E., and Ben-Tal, N. (2007) *J Biol Chem.* **282,** 37854-37863

17. Lagerstedt, J. O., Voss, J. C., Wieslander, A., and Persson, B. L. (2004) *FEBS Lett.* **578,** 262-268

18. Hubbell, W. L., Cafiso, D. S., and Altenbach, C. (2000) *Nat. Struct. Biol* **7,** 735-739

19. Langen, R., Oh, K. J., Cascio, D., and Hubbell, W. L. (2000) *Biochemistry* **39,** 8396-8405

20. Voss, J., He, M. M., Hubbell, W. L., and Kaback, H. R. (1996) *Biochemistry* **35,** 12915-12918

21. Zhao, M., Zen, K. C., Hubbell, W. L., and Kaback, H. R. (1999) *Biochemistry* **38,** 7407-7412

22. Ginalski, K., Elofsson, A., Fischer, D., and Rychlewski, L. (2003) *Bioinformatics.* **19,** 1015-1018

23. Schwede, T., Kopp, J., Guex, N., and Peitsch, M. C. (2003) *Nucleic Acids Res.* **31,** 3381-3385

24. Rotin, D. and Grinstein, S. (1989) *Am. J. Physiol* **257,** C1158-C1165

25. Pedersen, S. F., King, S. A., Rigor, R. R., Zhuang, Z. P., and Cala, P. M. (2003) *Biophysical Journal* **84,** 151A

26. Rasmussen, M., Alexander, R. T., Darborg, B. V., Mobjerg, N., Hoffmann, E. K., Kapus, A., and Pedersen, S. F. (2008) *Am J Physiol Cell Physiol* **294,** C197-C212

27. Meinild, A. K., Loo, D. D., Skovstrup, S., Gether, U., and MacAulay, N. (2009) *J Biol Chem.* **284,** 16226-16235

28. Nimigean, C. M. (2006) *Nat. Protoc.* **1,** 1207-1212

29. Accardi, A., Kolmakova-Partensky, L., Williams, C., and Miller, C. (2004) *J Gen. Physiol* **123,** 109-119

30. Froncisz, W. and Hyde, J. S. (1982) *J. Magnetic Resonance* **47**, 515-521

31. Hubbell, W. L., Froncisz, W., and Hyde, J. S. (1987) Review of Scientific Instruments **58**, 1879

32. Pao, S. S., Paulsen, I. T., and Saier, M. H., Jr. (1998) *Microbiol. Mol Biol Rev.* **62,** 1-34

33. Slepkov, E. R., Rainey, J. K., Li, X., Liu, Y., Cheng, F. J., Lindhout, D. A., Sykes, B. D., and Fliegel, L. (2005) *J Biol Chem.* **280,** 17863-17872

34. Counillon, L., Noel, J., Reithmeier, R. A., and Pouyssegur, J. (1997) *Biochemistry* **36,** 2951-2959

35. Altenbach, C., Oh, K. J., Trabanino, R. J., Hideg, K., and Hubbell, W. L. (2001) *Biochemistry* **40,** 15471-15482

36. Columbus, L. and Hubbell, W. L. (2004) *Biochemistry* **43,** 7273-7287

37. Mchaourab, H. S., Oh, K. J., Fang, C. J., and Hubbell, W. L. (1997) *Biochemistry* **36,** 307-316

38. Kowdley, G. C., Ackerman, S. J., John, J. E., III, Jones, L. R., and Moorman, J. R. (1994) *J Gen. Physiol* **103,** 217-230

39. Lu, L., Montrose-Rafizadeh, C., Hwang, T. C., and Guggino, W. B. (1990) *Biophys. J* **57,** 1117-1123

40. Shrode, L. D., Gan, B. S., D'Souza, S. J., Orlowski, J., and Grinstein, S. (1998) *Am. J. Physiol* **275,** C431-C439

41. Hilger, D., Polyhach, Y., Padan, E., Jung, H., and Jeschke, G. (2007) *Biophys. J* **93,** 3675-3683

42. Arkin, I. T., Xu, H., Jensen, M. O., Arbely, E., Bennett, E. R., Bowers, K. J., Chow, E., Dror, R. O., Eastwood, M. P., Flitman-Tene, R., Gregersen, B. A., Klepeis, J. L., Kolossvary, I., Shan, Y., and Shaw, D. E. (2007) *Science* **317,** 799-803

43. Galili, L., Herz, K., Dym, O., and Padan, E. (2004) *J Biol Chem.* **279,** 23104-23113

44. Kozachkov, L., Herz, K., and Padan, E. (2007) *Biochemistry* **46,** 2419-2430

45. Guo, Z., Cascio, D., Hideg, K., Kalai, T., and Hubbell, W. L. (2007) *Protein Sci* **16,** 1069-1086

46. Fajer, M. I., Li, H., Yang, W., and Fajer, P. G. (2007) *J Am Chem. Soc.* **129,** 13840-13846

47. DeWeerd, K., Grigoryants, V., Sun, Y., Fetrow, J. S., and Scholes, C. P. (2001) *Biochemistry* **40,** 15846-15855

48. Bolin, K. A., Hanson, P., Wright, S. J., and Millhauser, G. L. (1998) *J Magn Reson.* **131,** 248-253

FOOTNOTES

Acknowledgements: This study was supported by the National Institutes of Health Grant HL-21179 (to P.M.C.), the Danish National Research Council (to S.F.P.), the Swedish Research Council (to J.O.L.) and a Biocampus Scholarship from University of Copenhagen (to E.B.N.). We thank S. Grinstein, Hospital for Sick Children, Ontario, Canada, for the kind gift of AP-1 cells, C. Altenbach, Dept. of Ophtalmology at the Jules Stein Eye Institute, UCLA, LA, California for providing us with the Basephase program, and M. Landau, Tel-Aviv University, Israel, for providing us with the PDB file for their model. Cariporide was a kind gift from Sanofi-Aventis. Anni Bech Nielsen, University of Copenhagen, and Steven E. Anderson, UCDavis, are gratefully acknowledged for skilled experimental assistance.

The abbreviations used are: PaNHE1, *Pleuronectes americanus* NHE1; AtNHE1, *Amphiuma tridactylum* NHE1; hNHE1, human NHE1; TM, transmembrane; IL, intracellular loop; EL, extracellular loop; EIPA, 5'-(*N*-ethyl-*N*-isopropyl)amiloride; HOE, Hoechst type inhibitor; TM, transmembrane;; 3D, 3-dimensional; IL, intracellular loop; EL, extracellular loop; SDSL, site-directed spin labeling; EPR, electron paramagnetic resonance; DDM, *n*-dodecyl ß-D-maltoside; CaM, calmodulin.

Figure legends

Figure 1. Alignment of hNHE1 and NhaA

hNHE1 was predicted to be similar to the structure of NhaA by a number of well-established secondary structure and fold recognition methods at the MetaServer (25). The alignment of the sequences (14% identical residues and 23% conserved substitutions in the aligned regions) is from the joint evaluation of the outcome by the 3D-Jury system at the same server and by manual adjustments as detailed in Experimental Procedures. The predicted TM helices of NHE1 are visualized in gray (note the lack of fit for some loop regions).

Figure 2. Full structural model of the N-terminal region of hNHE1

The structure model is based on the known structure of the smaller bacterial Na^+/H^+ exchanger NhaA. The shown representations include the transmembrane domains only [Residues 15-31 (TM I), 104-123 (TM II), 130-147 (TM III), 160-179 (TM IV), 191-209 (TM V), 228-246 (TM VI), 255-272 (TM VII), 300-317 (TM VIII), 333-353 (TM IX), 417-437 (TM X), 453-473 (TM XI), and 481-502 (TM XII)] and exclude connecting loops and terminal extension. The color code used is light-blue for TMs I and II, dark-blue for TMs III, IV and V, green for TMs VI, VII, VIII and IX, and yellow for TMs X, XI and XII. A. Side-view of the hNHE1 structure in the plane of the lipid bilayer. B. Cytoplasmic view. The insert shows the numbering of the individual helices.

Figure 3. Solid surface structure representations of TMs III, IV, V, X, XI and XII (referred to as the catalytical core in the text) in the hNHE1 model

Positively charged residues are shown in blue, negatively charged residues in red, and polar residues in green. A. The cytoplasmic view (structure to the right in panel A is tilted 15° downwards compared to the structure to the left) and reveals a cavity (*arrows*) in the structure that reaches down to Arg^{425} (*brown arrow*). Several charged and polar residues that may be involved in the ion-translocation are located near this cavity. These include Arg^{458} and Arg^{500} (positively charged), Glu^{131} (negatively charged) and, Ser^{132}, Thr^{433}, Asn^{437} and Tyr^{454} (polar). B. The face of the protein exposed to the outside of the cell does not exhibit any obvious cavity in the structure. However, a cluster of charged residues (Asp^{470}, Lys^{471}, Lys^{472} and His^{473}) at the end of TM XI and also some scattered polar residues (e.g. Tyr^{209}, Thr^{417} and Thr^{482}) are accessible on the outside surface of the transmembrane domain. C. The side-view representation shows that primarily hydrophobic side-chains are pointed into the interior of the lipid bilayer. TMs I, II, VI, VII, VIII and IX are shown as grey ribbons for orientation (compare with Figure 2).

Figure 4. Structure of the Na^+/H^+ exchanger catalytical core

A. The central parts of TM domains IV, V, X and XI, the presumed catalytical core for hNHE1-catalyzed Na^+/H^+ exchange, are represented as a ribbon diagram. B. Schematic depiction of the central core of NHE1 (left) and NhaA (right). The amino acid side-chains suggested to directly participate in ion translocation are shown. The positions of the main spin-labels are shown in red in hNHE1. Note that the characteristic crossover by the extended structures of helices IV and XI results in energetically unfavorable dipole-dipole pairings (dipoles shown as $\delta+$ and $\delta-$) at the ends of the disrupted α-helices.

Figure 5. Functional evaluation of the NHE1 constructs in AP1 cells and liposomes

A-C. Regulation of intracellular pH (pH_i) after an acid load in AP1 cells expressing the $Ala^{173}Cys$ (A), $Ile^{461}Cys$ (B) or $Ala^{173}Cys/Ile^{461}Cys$ hNHE1. AP1 cells were loaded with BCECF and mounted on a Zeiss Axiovert S100 microscope. The cells were perfused with nominally HCO_3^--free HEPES buffered isotonic Ringer which, where indicated by the bar, additionally contained 10 mM NH_4Cl. Calibration to pH_i was carried out as previously described (12). Data shown are representative of 6-7 independent experiments per condition. The rates of pH_i recovery, obtained at similar starting pH_i values, but not normalized to expression levels, were 0.13 ± 0.010 ($Ala^{173}Cys$, n=7), 0.10 ± 0.0039 ($Ile^{461}Cys$, n=6) and 0.17 ± 0.0037 ($Ala^{173}Cys/Ile^{461}Cys$, n=6). D. Coomassie Fluor Orange staining and western blot of the $Ala^{173}Cys/Ile^{461}Cys$ hNHE1 mutant after purification. Purification, staining and immunoblotting were carried out as described in Experimental procedures. Coomassie Fluor Orange staining is shown on the left, and Western blotting for NHE1 on the right. 1: The solubilized membrane fraction before transfer to the Ni^{2+} column; 2: Eluate from Ni^+ column with Ni^+ elution buffer (containing 300 mM imidazole); 3: Eluate from the CaM column with CaM elution buffer; 4: Purified Ala173Cys/Ile461Cys hNHE1sample obtained from the concentration of the sample shown in column3. E-F. $^{22}Na^+$ uptake and H^+ flux by hNHE1 reconstituted in liposomes. E. $^{22}Na^+$ uptake was measured over time in hNHE1-liposome suspensions. Assays were performed in high osmolarity buffered sucrose solution and initiated by addition of tracer $^{22}Na^+$ containing solution. F.

hNHE1-liposomes were suspended in a poorly buffered KCl medium, monitored with a pH microelectrode in the external bath solution and expressed as H^+ flux. The H^+ flux reaction was initiated by adding 10 µl of 4M NaCl solution at the time indicated. Where indicated, liposomes were suspended in EVM in presence of 50 µM EIPA. The difference caused by EIPA represents the NHE1-specific flux.

Figure 6. EPR analyses of hNHE1 Ala^{173}Cys, Ile^{461}Cys, and Ala^{173}Cys/Ile^{461}Cys

The spectra were collected from samples of purified hNHE1 in CaM elution buffer (pH 7.5) containing 0.01% DDM, and the protein concentration (normalized to 20 µM spin for singles, 40 µM for double and sum of singles) is normalized to the same value for all samples. (A) Spin label positions (red) and functionally central residues (black) in hNHE1. See text for details. (B) Top: Effects of cariporide (0.1 mM) and low pH (5.1) on the EPR spectra of samples containing a spin label at position Ala^{173}Cys or Ile^{461}Cys, respectively. Bottom: Effects of cariporide (0.1 mM) and low pH (5.1) on the EPR spectra of double labeled Ala^{173}Cys/Ile^{461}Cys samples, and the signal from the double labeled sample compared to the sum of singles. Center in pink: signal from the cysteine-less hNHE1, which was incubated with spin label and examined at a concentration similar to the preparations containing a single- or double-Cys substitution (~20 µM NHE1). This background signal was subtracted from all spectra in panels A-D. Each spectrum shows a scan over a field of 100 G.

Figure 7. EPR analyses of paNHE1 Ala^{164}Cys, Ile^{452}Cys, and Ala^{164}Cys/Ile^{452}Cys

The spectra were collected from samples of purified paNHE1 in PBS buffer (pH 7.5) containing 0.01% DDM, and the protein concentration (normalized to 20 µM spin for singles, 40 µM for double and sum of singles) is normalized to the same value for all samples. (A) Spin label positions (red) and functionally central residues (blue) in paNHE1. See text for details. (B) Top: Effects of cariporide (1 mM) and low pH (5.1) on the EPR spectra of samples containing a spin label at position Ala^{164}Cys or Ile^{452}Cys, respectively. Bottom: Effects of cariporide (1 mM) and low pH (5.1) on the EPR spectra of double labeled Ala^{164}Cys/Ile^{452}Cys samples, and the signal from the double labeled sample compared to the sum of singles. The residual signal was subtracted from all spectra. Each spectrum shows a scan over a field of 100 G.

Figure 8. Effect of Arg^{425}Ala mutation on hNHE1 expression, localization and function

A. Recovery of pH_i after an NH_4Cl-prepulse-induced acid load in AP-1 cells stably transfected with wt hNHE1 (open circles) or Arg^{425}Ala hNHE1 (filled circles). Experiments were carried out essentially as described in the legend to Fig. 5, except that the measurements were carried out in a PTI fluorescence spectrophotometer. Where indicated, HEPES-buffered IR was replaced with NH_4Cl-containing and Na^+-free Ringer, respectively, as indicated by the bars. The graphs shown are representative of at least 3 independent experiments per condition. B. Summary of the experiments shown in A, showing the initial rate of pH_i recovery for wt hNHE1 and Arg^{425}Ala hNHE1, respectively. The insert shows the pH_i recovery rates corrected for the relative levels of wt and Arg^{425}Ala hNHE1 in the plasma membrane, calculated as described in Experimental Procedures. C. Confocal images of AP-1 cells transfected with wt hNHE1, Arg^{425}Ala hNHE1, or untransfected as indicated. Cells were paraformaldehyde-fixed, labeled for NHE1 followed by secondary, Alexa488-coupled antibody, and imaged using a Leica confocal microscope as detailed in Experimental procedures. Images shown are representative of at least 3 independent experiments per condition.

Figure 9. Tentative working model of ion translocation in the catalytic core of NHE1

The figure depicts possible conformational changes in the TM IV-TM XI crossover arrangement during NHE1 ion translocation induced by an acidic pH change. A. Charge compensation from Arg^{425} located in TM X stabilizes the energetically unfavorable negative/negative and positive/positive dipole-dipole pairings in the arrangement of the TM IV/TM XI helices. B. An acidic pH change results in alteration of the

protonation state of the region of TM IX located at the entrance of the proposed funnel, eliciting a conformational change in TM IX, which causes a direct contact between TM IV and TM IX (not shown). This rearrangement of TM IV results in a reorientation of TM IV and TM XI such that a Na+ binding site is exposed to the extracellular space. C-F. Binding of Na^+ causes a charge imbalance, triggering a movement of the TM IV and TM XI helices, exposing Na^+ to the cytoplasm. The release of Na^+ results in protonation of the Na^+ binding site, causing a conformational change leading back to the original arrangement of TM IV and TM XI.

Figure 1

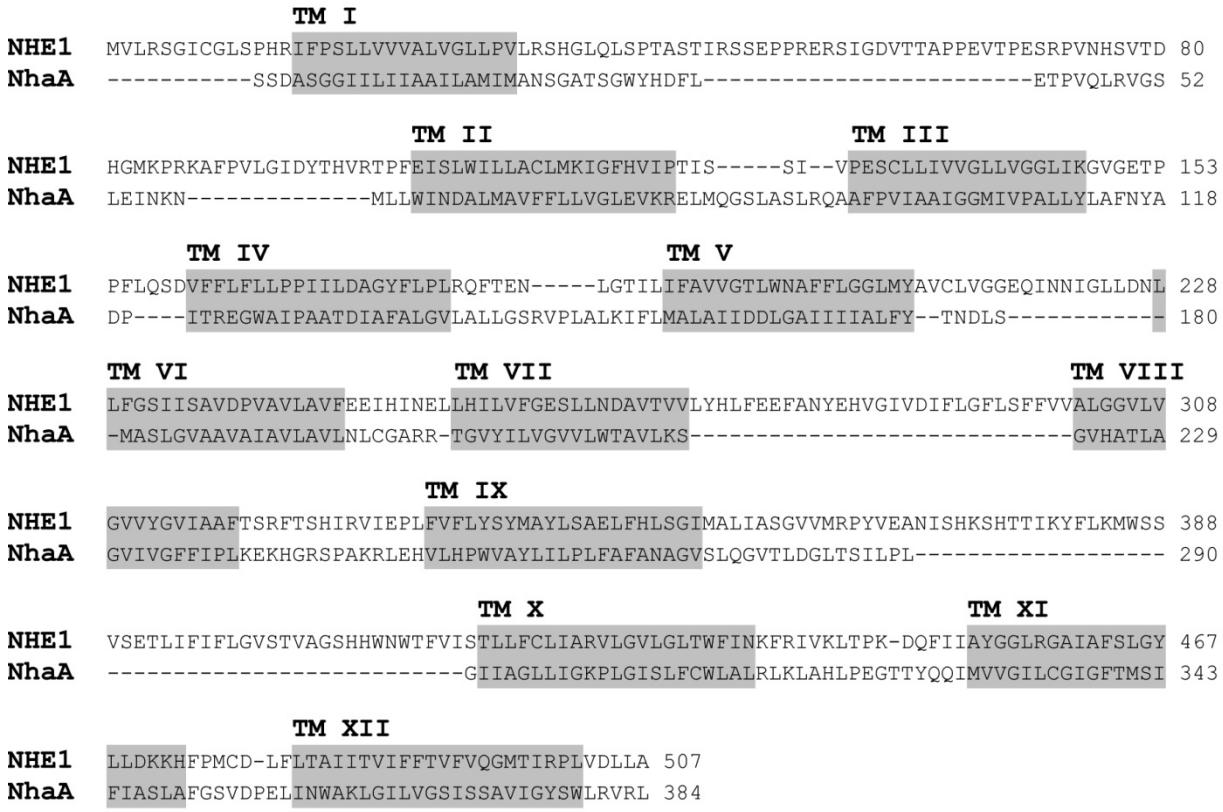
TM I
NHE1 MVLRSGICGLSPHRIFPSLLVVVALVGLLPVLRSHGLQLSPTASTIRSSEPPRERSIGDVTTAPPEVTPESRPVNHSVTD 80
NhaA ----------SSDASGGIILIIAAILAMIMANSGATSGWYHDFL----------ETPVQLRVGS 52
TM II
TM III
NHE1 HGMKPRKAFPVLGIDYTHVRTPFEISLWILLACLMKIGFHVIPTIS-----SI--VPESCLLIVVGLLVGGLIKGVGETP 153
NhaA LEINKN----------MLLWINDALMAVFFLLVGLEVKRELMQGSLASLRQAAFPVIAAIGGMIVPALLYLAFNYA 118
TM IV
TM V
NHE1 PFLQSDVFFLFLLPPIILDAGYFLPLRQFTEN-----LGTILIFAVVGTLWNAFFLGGLMYAVCLVGGEQINNIGLLDNL 228
NhaA DP----ITREGWAIPAATDIAFALGVLALLGSRVPLALKIFLMALAIIDDLGAIIIIALFY--TNDLS---------- 180
TM VI
TM VII
TM VIII
NHE1 LFGSIISAVDPVAVLAVFEEIHINELLHILVFGESLLNDAVTVVLYHLFEEFANYEHVGIVDIFLGFLSFFVVALGGVLV 308
NhaA -MASLGVAAVAIAVLAVLNLCGARR-TGVYILVGVVLWTAVLKS----------GVHATLA 229
TM IX
NHE1 GVVYGVIAAFTSRFTSHIRVIEPLFVFLYSYMAYLSAELFHLSGIMALIASGVVMRPYVEANISHKSHTTIKYFLKMWSS 388
NhaA GVIVGFFIPLKEKHGRSPAKRLEHVLHPWVAYLILPLFAFANAGVSLQGVTLDGLTSILPL---------- 290
TM X
TM XI
NHE1 VSETLIFIFLGVSTVAGSHHWNWTFVISTLLFCLIARVLGVLGLTWFINKFRIVKLTPK-DQFIIAYGGLRGAIAFSLGY 467
NhaA ----------GIIAGLLIGKPLGISLFCWLALRLKLAHLPEGTTYQQIMVVGILCGIGFTMSI 343
TM XII
NHE1 LLDKKHFPMCD-LFLTAIITVIFFTVFVQGMTIRPLVDLLA 507
NhaA FIASLAFGSVDPELINWAKLGILVGSISSAVIGYSWLRVRL 384

Figure 2

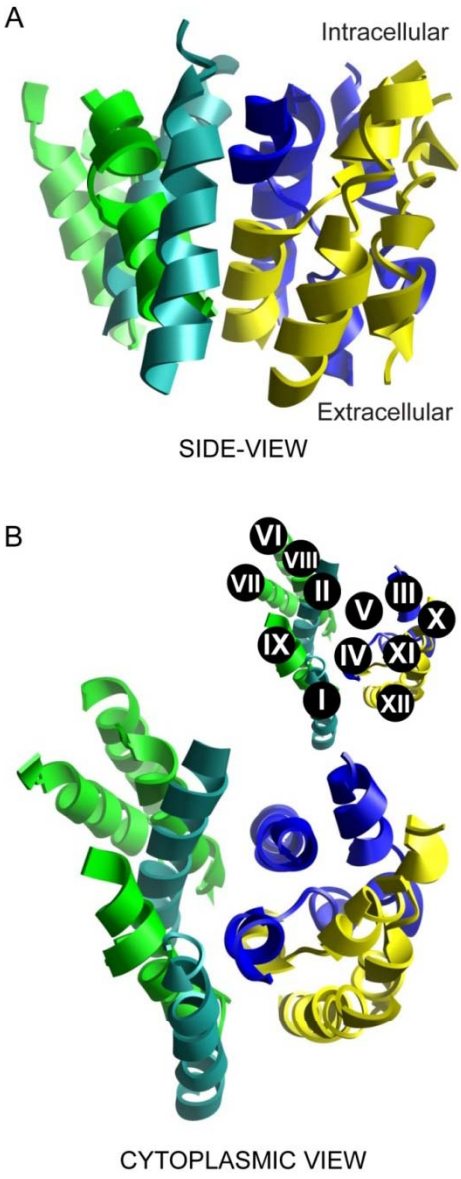
A
Intracellular
Extracellular
SIDE-VIEW
B
VI
VIII
VII
II
III
V
X
IX
IV
XI
XII
I
CYTOPLASMIC VIEW

Figure 3

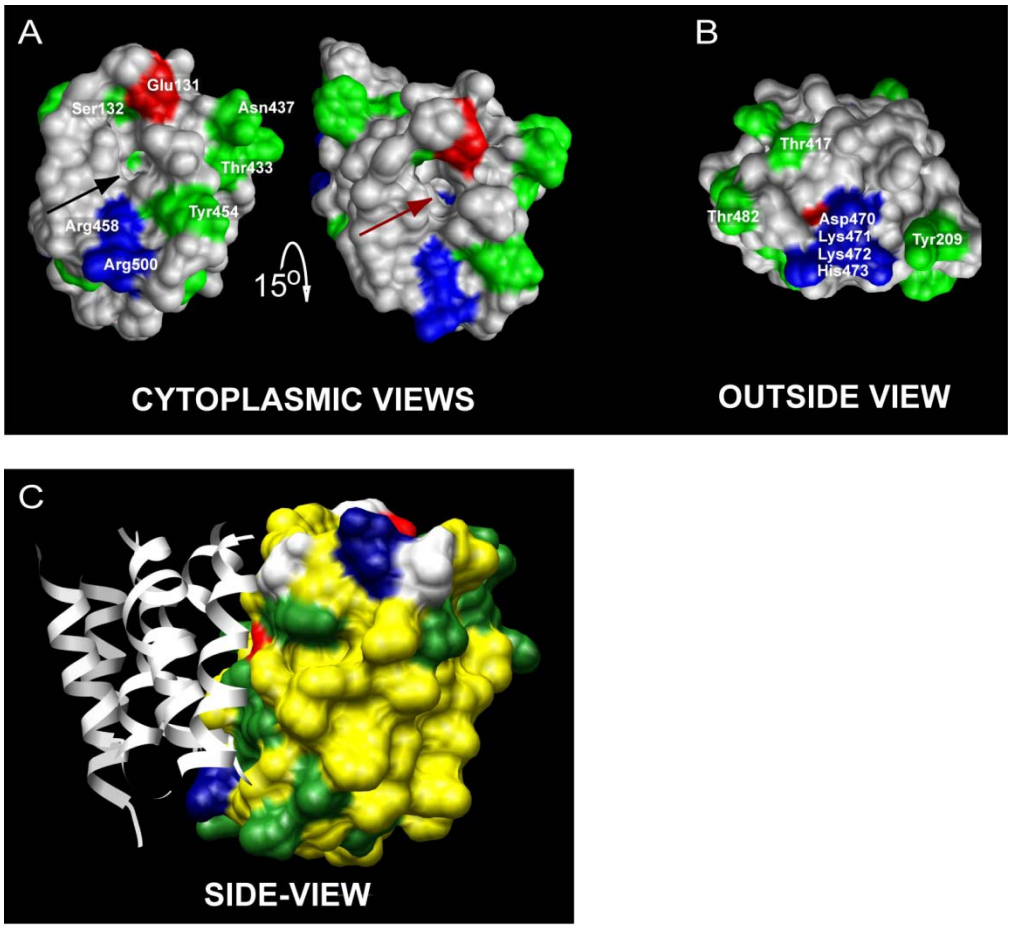
A
Glu131
Ser132
Asn437
Thr433
Tyr454
Arg458
Arg500
15°
CYTOPLASMIC VIEWS
B
Thr417
Thr482
Asp470
Lys471
Lys472
His473
Tyr209
OUTSIDE VIEW
C
SIDE-VIEW

Figure 4

A

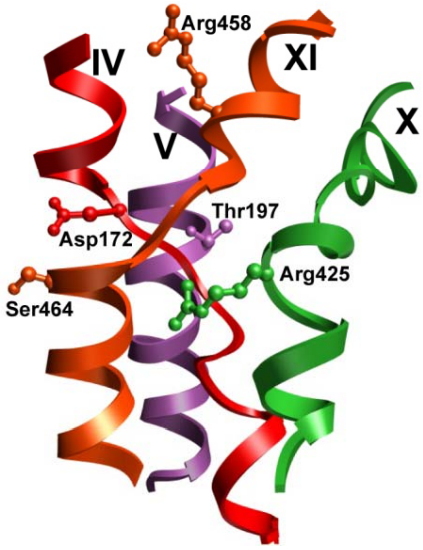
intracellular
Arg458
IV
XI
X
V
Thr197
Asp172
Arg425
Ser464
extracellular

B

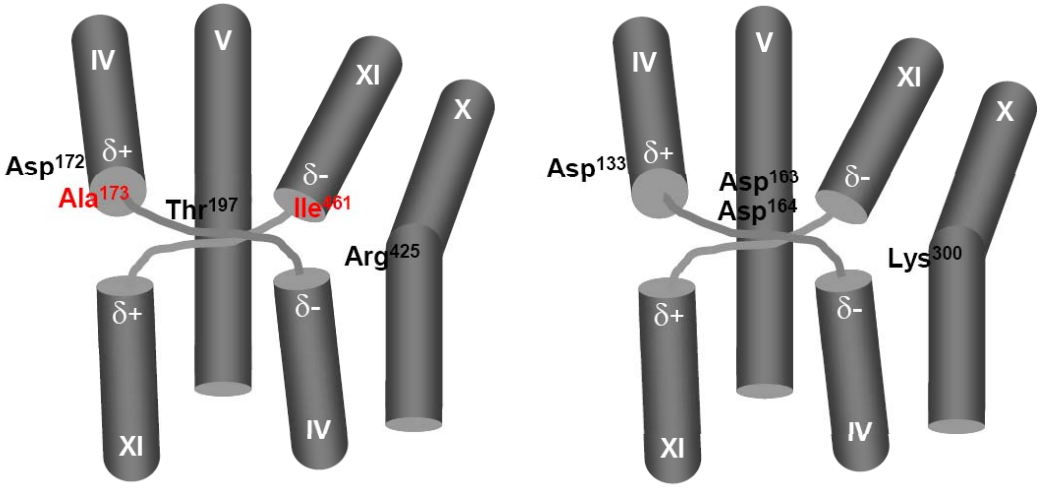
intracellular
IV
V
XI
X
Asp172
δ+
Ala173
Thr197
δ-
Ile461
Arg425
δ+
δ-
XI
IV
Asp133
Asp163
Asp164
Lys300
extracellular
hNHE1
NhaA

Figure 5

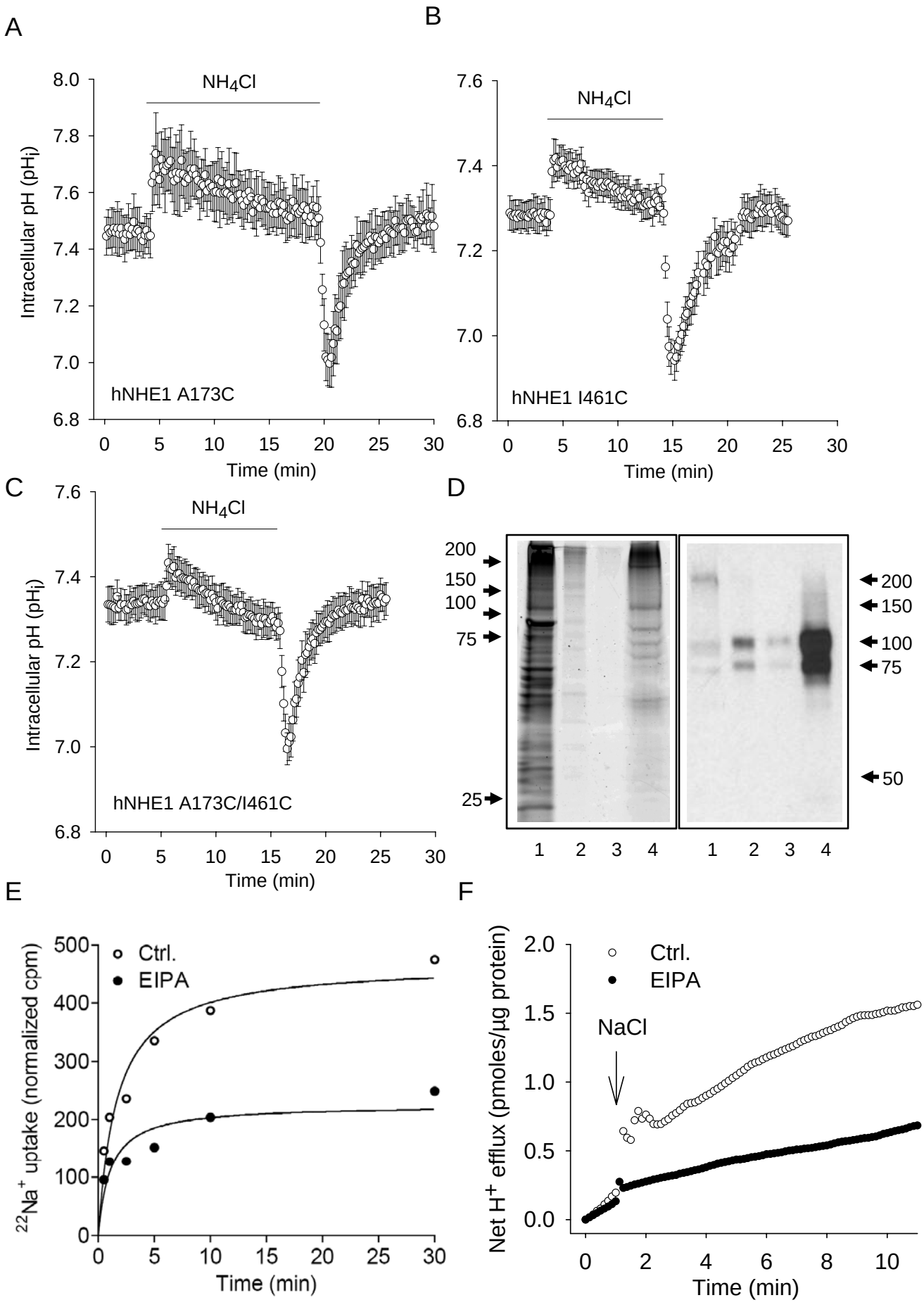
A
B
C
D
E
F
NH4Cl
Intracellular pH (pHi)
hNHE1 A173C
hNHE1 I461C
hNHE1 A173C/I461C
Time (min)
200
150
100
75
50
25
1 2 3 4 1 2 3 4
22Na+ uptake (normalized cpm)
Ctrl.
EIPA
NaCl
Net H+ efflux (pmoles/µg protein)

Figure 6

A

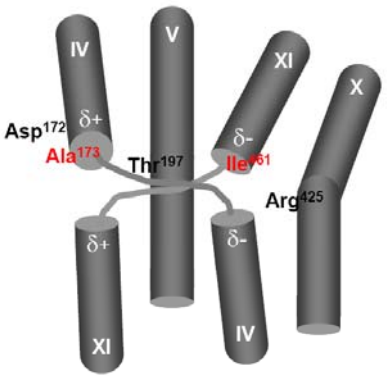

Spin label positions (red) and functionally central residues (black) in hNHE1

B

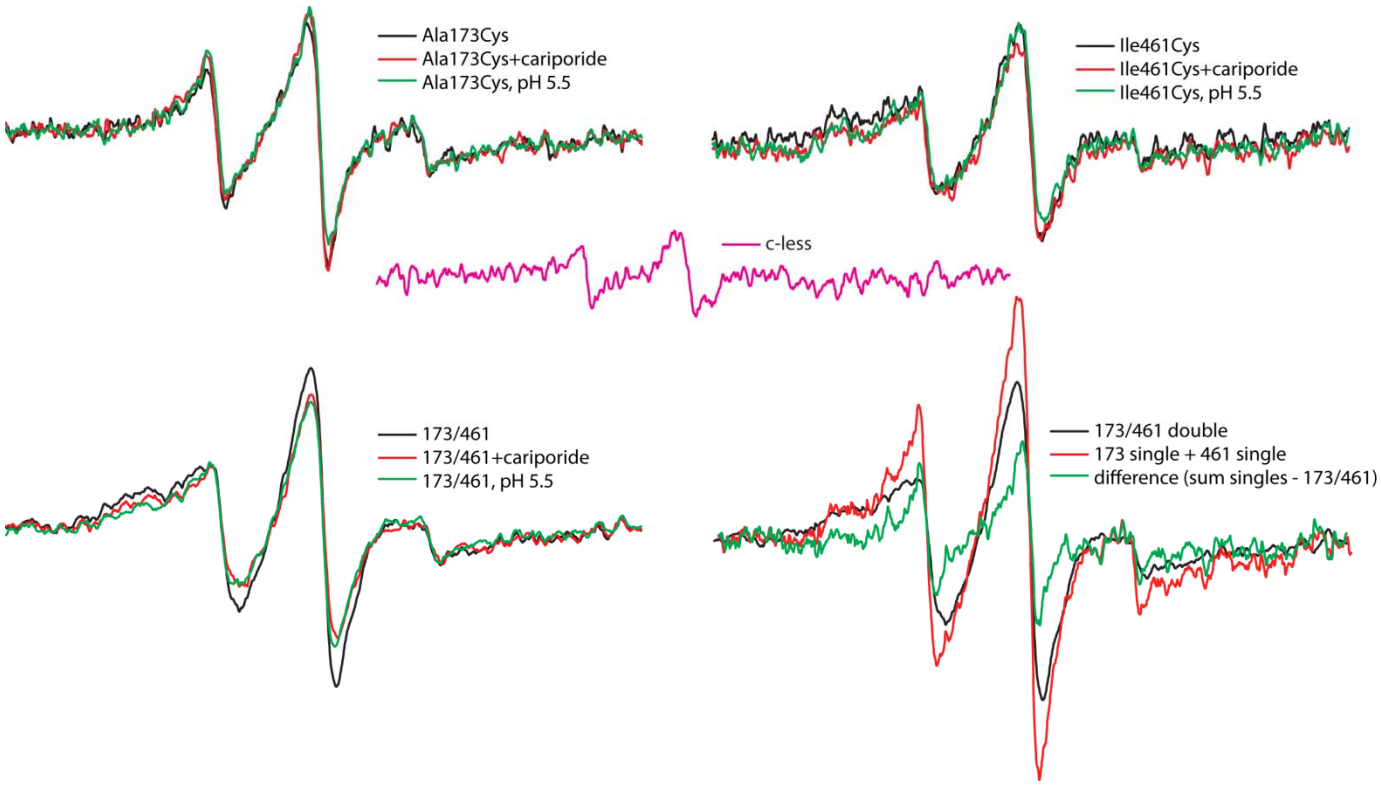

Figure 7

A

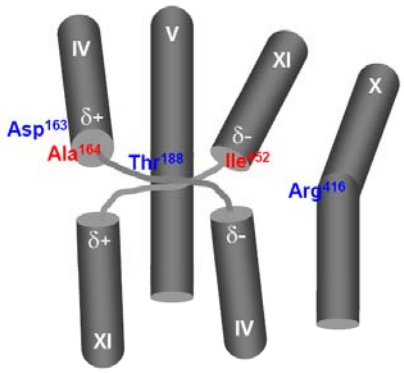

Spin label positions (red) and functionally central residues (blue) in paNHE1

B

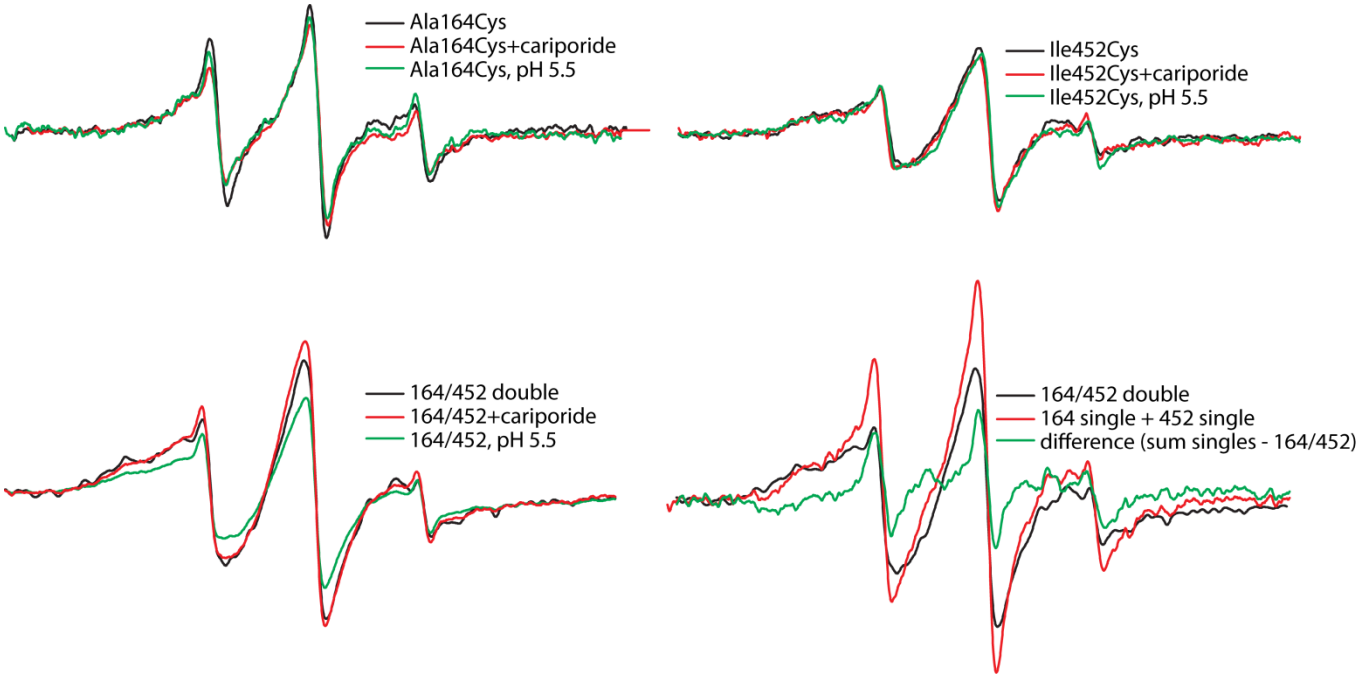

Figure 8

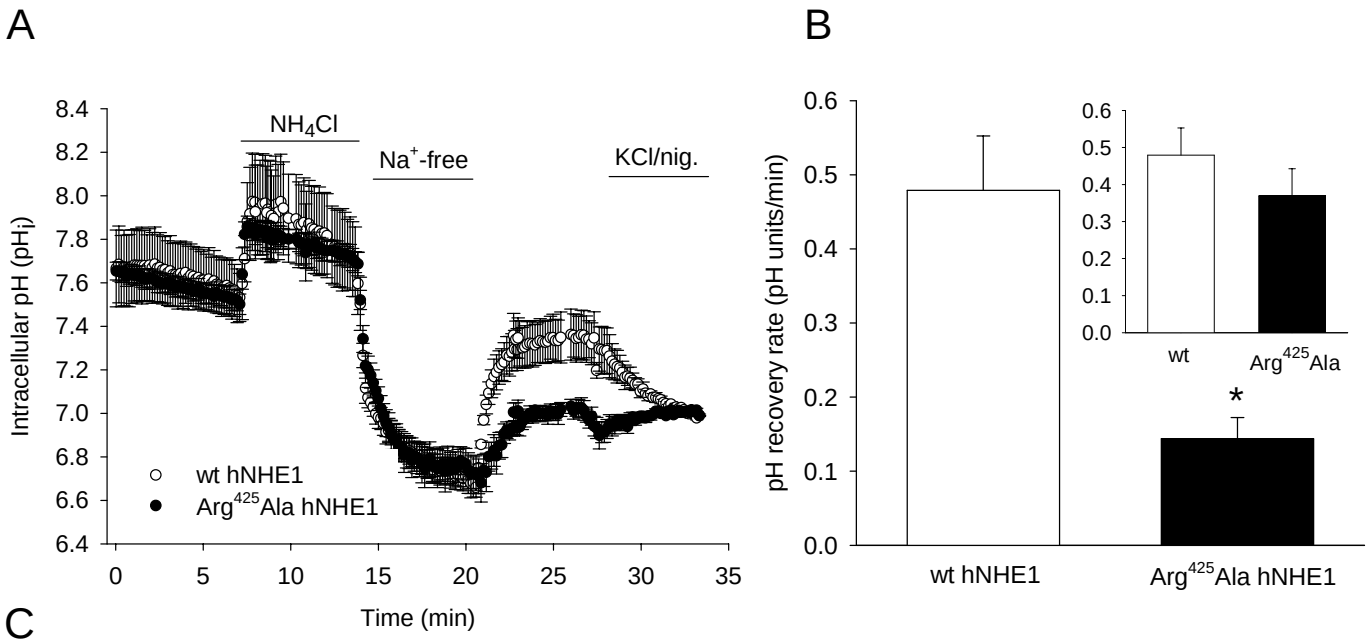
A
B
NH4Cl
Na+-free
KCl/nig.
Intracellular pH (pHi)
Time (min)
wt hNHE1
Arg425Ala hNHE1
pH recovery rate (pH units/min)
wt
Arg425Ala
*
wt hNHE1
Arg425Ala hNHE1

C

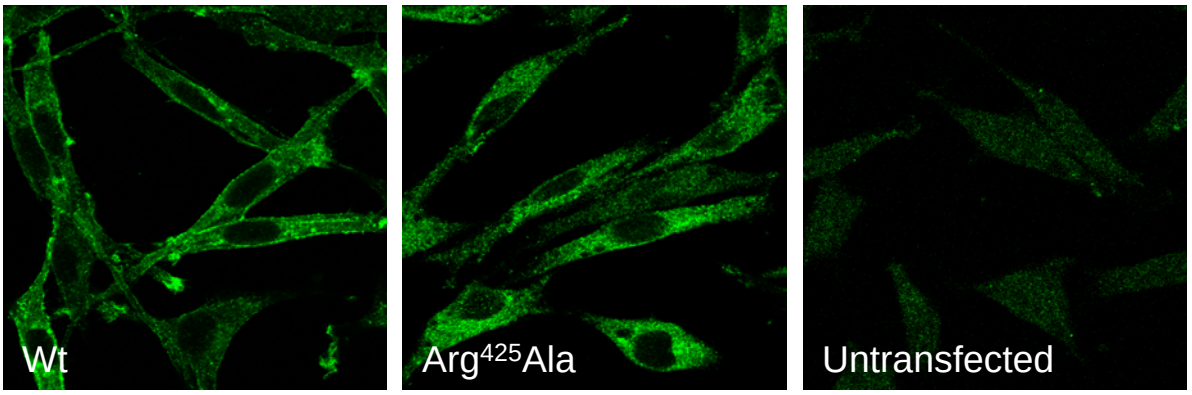
Wt
Arg425Ala
Untransfected

Figure 9

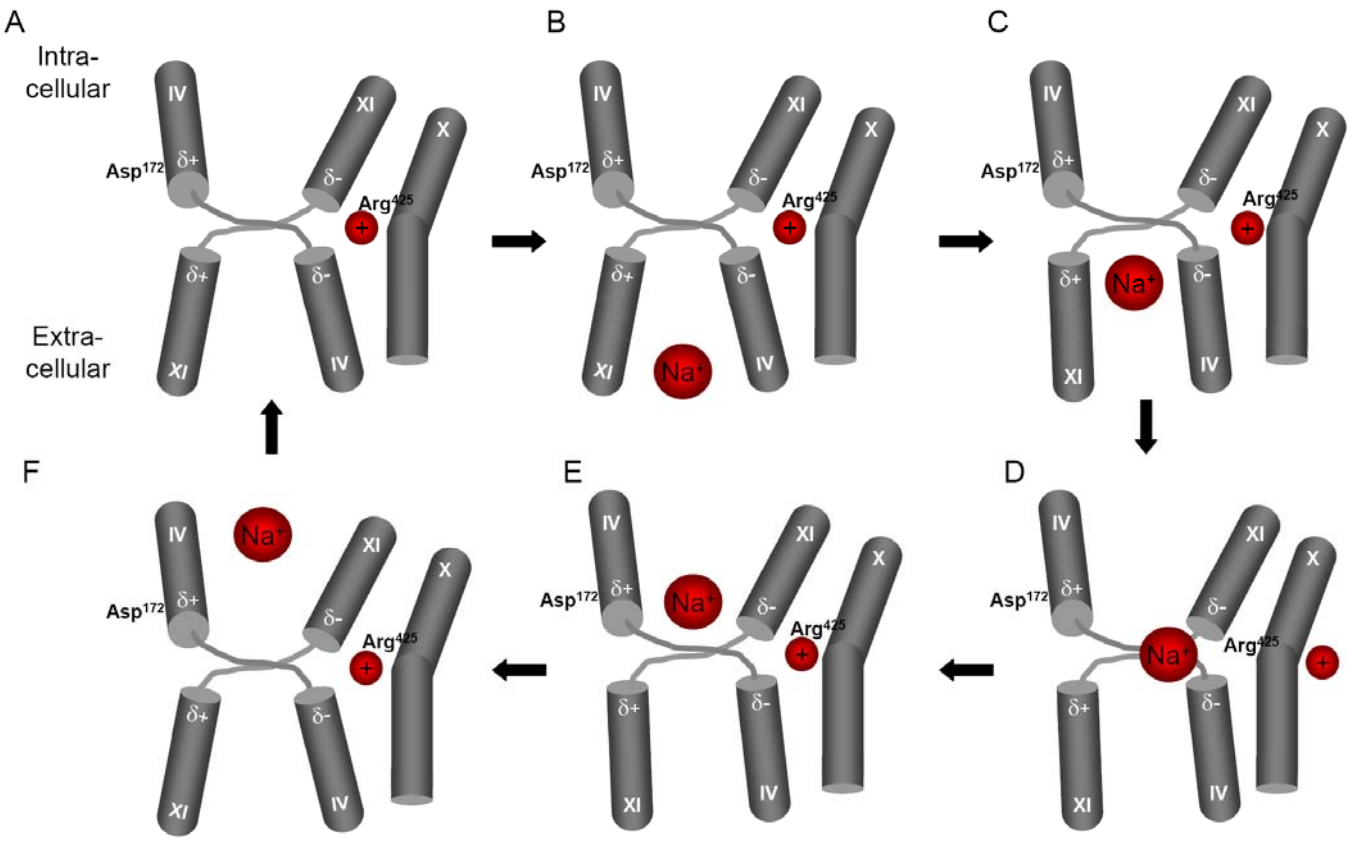
A
Intra-
cellular
Extra-
cellular
IV
XI
X
Asp172
Arg425
δ+
δ-
Na+
B
C
D
E
F

Supplementary material

Suppl. Fig. 1. Effect of cariporide on hNHE1 activity in AP1 cells.

AP1 cells stably transfected with hNHE1 were loaded with BCECF-AM and pH_i assessed as described in Experimental Procedures. NHE1 activity was assessed as recovery after an NH_4Cl prepulse-induced acid load, using fluorescence microscopy and digital image analysis.

Suppl. Fig. 2. Current measurements after Arg^{425}Ala hNHE1 expression in Xenopus oocytes

Xenopus oocytes were either water-injected (A) or injected with Arg^{425}Ala hNHE1 (B). The I/V relations were determined under six different conditions: in NaCl buffer, pH 7.4 (white circles), in NaCl buffer, pH 5.8 (gray circles), in NaCl buffer with EIPA, a NHE1 blocker (black triangles), after acidic pre-incubation at pH 5.8 in NaCl buffer pH 7.4 (red triangles), after pre-incubation at pH 5.8 in NaCl buffer, pH 5.8 (blue squares), and after pre-incubation at pH 5.8 in NaCl buffer with EIPA (green squares). The I/V plots are the mean of six oocytes from two different donor frogs. The lines are connections of actual data points.

Supplementary Fig. 1

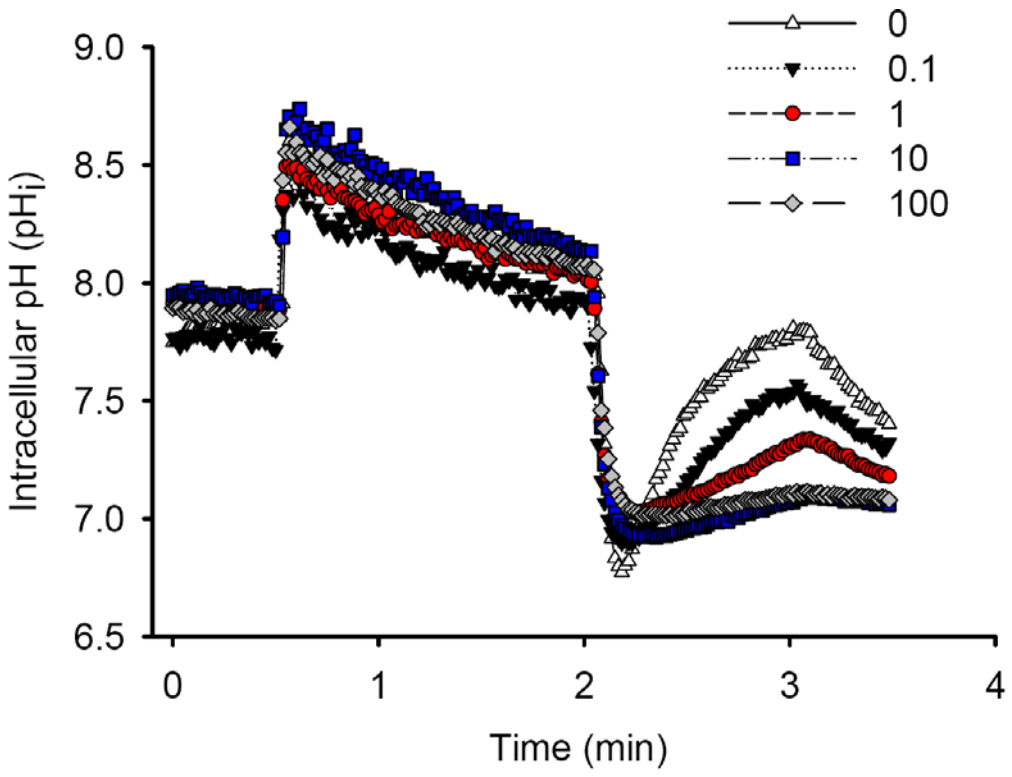

Supplementary Fig. 2